Development of crane for additive manufacturing

Lazar Milovic

DIVISION OF PRODUCT DEVELOPMENT | DEPARTMENT OF DESIGN SCIENCES
FACULTY OF ENGINEERING LTH | LUND UNIVERSITY
2018

MASTER THESIS

Development of crane for additive manufacturing

Lazar Milovic

LUND
UNIVERSITY

Development of crane for additive manufacturing

Published by
Department of Design Sciences
Faculty of Engineering LTH, Lund University
P.O. Box 118, SE-221 00 Lund, Sweden

Subject: Machine Design for Engineers (MMKM05)
Division: Division of Product Development
Supervisor: Giorgos Nikoleris
Examiner: Olaf Diegel

Abstract

Increased popularity of additive manufacturing has pushed the method into new areas where it has not been used before, such as construction. Buildings are being 3D printed by various companies around the world, but the application of additive manufacturing in construction is still in its early stages. In order to conduct research in this field, the Department of Design Sciences at Lund University are in need of a crane to carry a cement extruder.

A crane was designed using readily available parts from the workshop at IKDC, which included a vertical beam used as the base, a horizontal beam with rails and a robot which could traverse on the rails. The crane can rotate around its vertical axis and it can also move linearly in the vertical and horizontal directions. Some of the parts where modified in the design process to better fit the expectations needed to complete their task, but the design was restrained from too big changes in order to reduce manufacturing costs.

Complete calculations were made on bearings, transmission unit and the overall structure, for dimensioning purpose and to ensure that failure will not occur during operation. Three types of methods were used for the structural analysis of the crane, an analytical method derived from Euler-Bernoulli beam theory and classic solid mechanics, a FEM method using CALFEM in MATLAB and a FEM simulation using ANSYS. A 3D model of the proposed design was created in CAD using SolidWorks.

Keywords: Additive manufacturing, construction, robotics, machine design, heavy industry

Sammanfattning

Användning av tillsatsframställnings metoder i byggbranschen har nyligen tagit fart och det finns redan företag som bygger hus på detta sätt. Däremot är applicering av metoden relativt ny inom byggnadskonstruktion och ytterligare forskning måste göras inom området. Institutionen för designvetenskaper vid LTH, Lunds Universitet, är därför intresserade av att tillverka en maskin som kan användas för 3D-printing av betong.

En kran tillverkades för detta ändamål, av delar som redan fanns i verkstaden på IKDC. Delarna som var tillgängliga inkluderade en stor vertikal balk som skulle användas som bas, en horisontell balk med spår och en platta utrustad med två motorer som kan röra sig på balkens spår. Kranen möjliggör rörelse i horisontell och vertikal led, samt rotation kring den vertikala axeln. Några av delarna var tvungna att modifieras för att möta kraven, men dessa förändringar var begränsade i avsikt att förhindra stora tillverkningskostnader.

Fullständiga beräkningar gjordes för dimensionering av kullager och rem för överföring av moment. Vidare gjordes hållfasthetsberäkningar för hela strukturen, i avsikt att förhindra brott i kranen eller att delar inte fungerar. Hållfasthetsberäkningar gjordes baserat på tre olika metoder, nämligen Euler-Bernoullis balk teori, CALFEM som är ett FEM verktyg i MATLAB och simulering med hjälp av ANSYS programvara. Lösningsförslaget för kranen modellerades med hjälp av CAD och presenterades i from av en 3D figur.

Nyckelord: Tillsatsframställning, byggnadskonstruktion, maskinkonstruktion, robotik, tung industri

Acknowledgments

I wish to express my gratitude to some people without whom this work would not have been possible.

I would like to thank my supervisor, Giorgos Nikoleris, who came up with the idea for this thesis, who answered my questions and gave me thoughtful input and comments on my work. Without your help I would have been clueless about what to do.

Thank you, Per-Erik Andersson for your counsel about the deformation constraints and for helping me check my results.

Thank you, Axel Nordin for checking the boundary conditions in ANSYS when I thought my simulation was wrong.

I would like to thank Josef from the workshop at IKDC who helped me find a tool for removing the axis after it has been placed in the beam.

I wish to also thank Bert Sjögren for helping me transfer my courser, without your help I would not have been able to do this thesis at this time. Also, special thanks to Per Lidström for his inspiration and even though I failed dynamics in the first try, you helped me turn this subject into one of my strong points. I hope the both of you enjoy your retirement.

Lastly, I wish to express my gratitude to my friends and family for their support through the course of this thesis.

Lund, June 2018

Lazar Milovic

Table of contents

List of acronyms and abbreviations

AM	additive manufacturing
CAD	computer aided design
COG	centre of gravity
cw	clockwise
DOF	degrees of freedom
EN	European norms
FEM	finite element method
FDM	fused deposition modeling
IKDC	Ingvar Kamprad’s design centrum
LTH	Lunds tekniska högskola

1 Introduction

1.1 Background

Additive manufacturing (AM) has become increasingly popular in the product development and product manufacturing process due to the low manufacturing costs and time. AM has mostly been used in relation with polymeric materials, due to the ease at which these materials can be manipulated in the AM process, and thus the application of this method has often been limited to products consisting of polymers. However, there is an interest to increase the scope of things which can be manufactured using AM, with other materials than polymers. Recently extruders capable of using concrete or cement as a construction material [1;2;3] have become available and thus enabling AM to occur at a larger scale. This large-scale additive manufacturing in turn requires larger robots and cranes on which these heavier extruders can be placed.

1.2 Aim and purpose

The main purpose of this paper is the development of a crane which will be used in AM for constructions using concrete or cement. The crane is developed from parts which are available in the workshop at Ingvar Kamprad design Centre (IKDC) at the faculty of engineering, Lund University (LTH) campus. These parts consist of a beam which can be fastened vertically to the floor and a model ZP-I linear gantry robot made by Güdel [4]. The beam which forms the foundation will often be referred to as the vertical beam, while the Güdel beam will be referred to as the horizontal beam, because cranes usually take the shape of a capital gamma letter Γ. The aim is to propose a design which could be assembled and would result in a crane capable of holding an extruder. It will be possible for the crane to move in two linear directions and rotate around its own axis, where the linear motion occurs along the vertical and horizontal axis, z- and y-axis respectively. As the designer of a machine, it is important to state the specifications for operation of the same machine, so that others might use it. It should also be noted that the aim of this thesis does not include the development of the extruder, it is assumed that such an extruder is readily available.

It is noteworthy to mention that the specifications put on the crane are requested by Associate Professor Giorgos Nikoleris, from the department of design sciences at LTH. He is also the supervisor of this thesis and the man behind the idea to design this crane.

In order to organize the stated problem a clear structure is proposed where the problem is divide into two phases, which are solved in numerical order. The first phase involves the vertical beam and how the horizontal beam is fastened to it which allows rotation around the vertical axis. In the second phase the horizontal beam is considered, the main problem in this phase involves structural design and identification of stresses and deformations which are to be kept at a minimum.

It is also important to bear in mind how the parts of the crane should be assembled and dissembled. This process will not occur often but is important in case of repairs or transport of the crane.

1.3 State of the art

In this section the state of the art for additive manufacturing used in construction will be presented. AM is related to an automatized manufacturing process where a computer aided design (CAD) file is used as an instruction for a robot driven extruder to recreate the same object. It should however be noted that automatization in construction exist in other forms than AM, such as automatized brick-laying, but such methods will not be discussed in depth here. This section is preserved for the recent technology in cement extruders and 3-D printed buildings.

1.3.1 **Small scale to large scale manufacturing**

There are currently three methods used for 3-D printing cement; D-Shape, Contour Crafting and Concrete Printing. D-Shape uses a powder deposition process where selected areas are hardened using a binder material, the final shape has to be dug out of the powder bed. Contour Crafting and Concrete Printing are based on similar methods where a wet cement material is pushed out a nozzle, controlled by a robotic arm for precision placement of the material in a 2-D plane. The difference is that Contour Crafting uses a trowel which helps guide the placement of material and results in a smooth surface, whereas in Concrete Printing more 3-dimensonall freedom is achieved by having a smaller resolution of disposition, as mentioned by Lim et al. [5]. Parallels, between these methods and traditional 3-D printing methods used in small scale AM, are drawn by Wu et al. [6], where the D-Shape and Concrete Printing methods are similar to inkjet powder printing and fused deposition modeling (FDM), respectively. In this case the Contour Crafting method has no equal and is consider its own category.

Furthermore, the same author has concluded that the benefits gained from small scale AM can be applied to a larger scale AM used in construction. Some of these are the reduced manufacturing cost, less spill material (except for the case of D-Shape), shorter manufacturing times and increased customization of the final product. This would allow construction companies to build both a series of building or an equal number of custom designed buildings, at the same rate.

The main problem related with transferring the technology from a small scale to a larger one, is related to the material used in the manufacturing and the robots used for controlling the manufacturing process. Material used in an AM process, especially if it is FDM, needs to satisfy certain characteristics, the material must be soft and formable when being pushed out of the nozzle, but should dry and solidify in time before the next layer is applied. At the same time, the material has to fulfill the criteria necessary for it to be used as a component in buildings. The robots have to be able to carry it all and maneuver freely in the 2-D space required to manufacture the desired building. [6, 7].

Considering the material aspect, the problem with finding a suitable material has usually been solved with using wet concrete in the nozzle. Some companies have their own recipes for suitable materials which usually involve improving the characteristics of concrete by adding glass fibers in the mix, as done by WinSun [8].

For the robotics problem, different types of solutions can be used, ranging from gantry type robots which occupy the whole design space, to one armed robots with several degrees of freedom (DOF). The idea is to attach one extruder at the endpoint tip of the robot arm which then moves according to the instructed pattern. These robots are often very large and can take the size of a building but smaller versions can be made when it is not necessary to manufacture tall buildings, as concluded by Labonnote et al. [7].

The same author writes about another approach in which many small robots are used to perform the task, called “swarm approach”. There are three different robot types which constitute the swarm, foundation-, grip- and vacuum robots. The foundation robot builds the base and the grip robots build the frame of the building, including the horizontal layers such as ceiling and roof. Lastly, the vacuum robot reinforces the structure by applying additional material to the areas created by the previous two, which is done by holding on the previous material by a suction cup, creating a vacuum grip. This method requires a prior mapping of the surface where the manufacturing should be performed, but according to Labonnote et al. it can be done with no human supervision, thus proving useful for application where it could be dangerous for humans to venture such as the site of a nuclear disaster.

1.3.2 **Printing a house**

The first house constructed using AM was completed in 2014, in China, done by the Chinese company specializing in 3-D printing buildings called WinSun [2;8]. The building was however not printed on site, but the parts which constitute the building were printed at the company's facility using their own composite as construction material. The parts were then delivered and assembled on site. After their milestone project, the company went on to construct several other residence houses and at their homepage it can be seen that their products are used in several landmark buildings across China.

Recently, a Danish company created the first house using AM technology on site, which also fulfills the regulations regarding residential buildings in the European Union (EU) [1]. Another European project related to on site AM, mentioned in [6] and [7] is the construction of a "canal house" in the Netherlands. The house is supposed to be quite complex with different themed rooms, which will all be constructed using AM. However, it is unclear when this project will finish.

The projects mentioned above all include the process of using AM technology to create a house, either by manufacturing the whole building on site or creating components at a facility. What these projects have in common is that the AM technology is restricted to only creating one element of the building, such as the walls and ceiling, which can usually be done using concrete. But a fully functional modern house needs to have plumbing, electricity, insolation and not to mention doors and windows. These elements must be added in various ways, which have to be incorporated into the AM process. According to [6;7;9], there is no smooth way to achieve this and there might be complications with every method. With this in mind, there is no need to separate on-site manufacturing from parts created in a factory, since both will have to be assembled in the end.

It is also noteworthy to mention that solutions presented by these companies are mostly based on the Contour Crafting method described in section 1.3.1, in combination with a gantry robot [3]. As can be noticed, the D-Shape method does not appear in any of the solutions, the amount of spill material relate to this method might be reason for this.

1.4 Scope

With the problem defined in the previous section, the scope of this thesis is clear; to develop a crane used for AM and state the specifications for the crane. The development process will apply knowledge from disciplines which fall under the broader subject of mechanical engineering, such disciplines include; solid mechanics, transmission mechanics and machine design.

The layout of this paper will be explained next, first the methods used to solve the stated problem are introduced, followed by the theory behind them. Next, a presentation of the result from the calculations done on the structure and the final design. The last chapter is dedicated to a discussion about the obtained results and a summary of the work done.

2 Method

2.1 Selection Method

As previously mentioned, the problem is divided into two phases, where similar methods will be used for each phase. This was done to divide the workload into smaller parts which can be solved separately without having to consider all the factors at once. This method works also as a checklist and even though there are only two points, they can easily be checked to ensure everything has been done. The proposed solution for each phase must be plausible, this is checked by considering manufacturing, assembly and disassembly. If a solution is too complicated to manufacture in an affordable way, or by conventional methods, it is not considered plausible. Likewise, if there is no reversible way to assemble the crane, the solution is not reasonable.

The proposed solution should not differ too much from the original design, some parts will be remade according to what is necessary for the crane to endure an applied load. This condition is interlinked with the previous; considering a simple and cheap solution, since too many alterations of the original design will be expensive and possibly difficult to manufacture. The crane is also required to move in two linear direction and rotate around its vertical axis, these aspects are included in the two phases, where the first phases focuses on the rotary motion and the second phase on the linear motion.

It has already been mentioned that the specifications are requested by Assoc. Prof. Giorgos Nikoleris, therefor a direct approach was chosen where no further investigation was done in order to specify further needs. The reason behind this is that the professor is considered as the user.

2.2 Process

After a plausible solution is found, according to the criteria's stated above, an analysis is conducted to find out if the solution can be applied without failure. First a motion analysis is done to understand how the moving parts operate, forces and torques are calculated. Then an analysis is done regarding the transmission of motion, this part includes the choice of transmission type and the placement of

motor drivers. Finally, when all necessary parts are in place, an analysis is done from a solid mechanics point of view to identify deformations and stresses in the parts.

2.3 Tools

The calculations will mostly be done analytically, by hand, especially when the mechanics and transmission parts of the problem are considered. These problems are capable of being solved by basic knowledge in mechanics. However, the solid mechanics part might be trickier due to the complexity of the geometry considered. If the geometry is complex, the deformation conditions might not be completely clear and further complications are introduced when a beam is considered instead of a bar. Thus, the aid of numerical methods available through commercial software will be used such as the finite element method (FEM). FEM will however be used in conjunction with analytical methods, this provides crosscheck of validity for the solution obtained by both methods.

It should be mentioned that three steps are used in the crosscheck of answers obtained in the structural analysis. The first step is using ANSYS software for the FEM analysis, this a completely numerical method which uses data from CAD files. The second method can be called "semi-analytical" and is based on using CALFEM, a MATLAB FEM tool [10], to calculate the reaction forces and moments, which are then put into the analytically derived formulas, being the final step, to obtain the maximum stresses and deformations. All three methods can check the validity of the other two, and CALFEM acts as a bridge since it has the possibility to provide the result in the form of point forces and moments, which is the way forces and moments are usually portrayed in analytical methods.

As previously mentioned, a CAD software will be used to model the parts of the plausible solution.

3 Theory

3.1 Kinetics

The dynamics are studied in order to obtain knowledge about the necessary torques required to move parts. For the beam and robot from Güdel, data about motor torques, robot velocity, acceleration and more, can be obtained from their product catalogue [4]. Therefor it is not necessary to calculate these, which further implies that the only dynamic calculations should be done for the rotary motion around the vertical z-axis.

From the equation of motion for plane motion, torque is given by;

$$\tau = I\dot{\omega} \tag{3.1}$$

where τ is the torque, I the inertia of the body and ω the angular velocity, the dot represents time derivative, time derivative of the velocity is acceleration, thus it is the angular acceleration. Inertia is defined as;

$$I = \sum m_i \rho_i^2 \tag{3.2}$$

where m_i is the mass of a particle in the body, and ρ_i the distance from the point of rotation to centre of gravity (COG), of the particle. This expression can be simplified by writing the total mass of the body as the sum of all particle mases, and setting ρ as the distance from the point of rotation, to the COG for the whole body. If the point of rotation is a fixed point, this expression can be simplified further. In the case of the crane, rotation occurs around one stationary axis, thus with the preceding discussion in mind, 3.1 is rewritten as;

$$\tau_O = I_O\dot{\omega} \tag{3.3}$$

The subscript O denotes that the torque and inertia are located around the same stationary point or axis in the reference frame. What equation 3.3 formulates is that if the inertia and angular acceleration around a stationary point or axis is known, then the torque around this same axis can be calculated.

This leads to the important introduction of Steiner's Theorem, which states that if the inertia around the COG is known, then the inertia around any parallel axis, P, can be calculated using the following expression;

$$I_P = I_G + md^2 \tag{3.4}$$

Where d is the distance between the COG axis and the new axis *P*. This can later be applied to any axis parallel with the previous one, thus the inertia around any arbitrary axis in the reference plane, can be calculated if the inertia around one axis, in the same plane, is known. The expressions used here can easily be found in any mechanics textbook, such as the one by Meriam & Kraige [11].

3.1.1 **Torque calculations**

Without the knowledge of how the final design will look like, a general formulation of the inertia can still be made. The torque calculations are related to the first phase, since the kinetics of the second phase are already known, thus this phase should be solved before the exact shape of the second part has been decided. But as will be shown, this can be done by simple approximations which will turn out to be correct even for the final result.

It is obvious that the final design will have a vertical axis, to which a horizontal beam is attached. To minimize the deformations at the endpoint of the horizontal beam, it is logical to place some kind of reinforcement, a diagonal beam is placed as support, creating the angle α between the two beams. Finally, a load can be hoisted up and down at the end of the horizontal beam. The stationary axis of rotation is placed through the centre of the physical axis. Figure 1 shows the structure described above, with the corresponding dimensions drawn out.

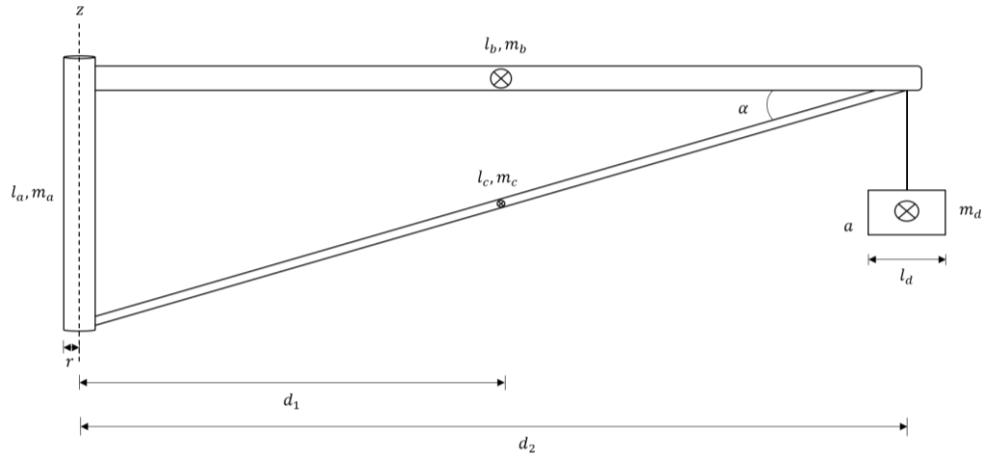

Figure 1. Approximation of how the final design might look like which is used to calculate the inertia around the axis of rotation. This axis is labelled with z in the figure. Lengths, masses and the distance from the COG to the z-axis are shown.

This structure can be divided into several parts, and the problem then becomes finding the inertia related to each part. The total inertia is the sum of the inertias

from each part, where the parts have been labelled from a to d, thus length l_a and mass m_a are the length and mass of part a. The inertia is calculated at the COG of each part and is derived using formulas for simple geometric objects, shown in figure 2, where beams are modelled as rectangular parallelepipeds and the axis is a cylinder.

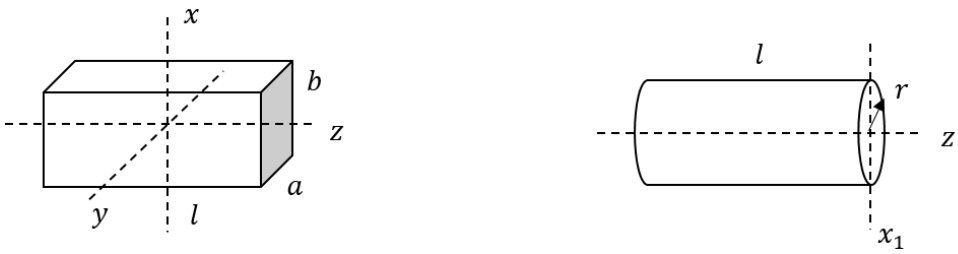

Figure 2. Dimensional properties of simple geometric bodies such as the rectangular parallelepiped and cylinder, used to calculate the inertia for these bodies.

From the definition of inertia, see Meriam & Kraige [11], the following results are derived for the rectangular parallelepiped;

$$I_{xx} = \frac{1}{12} m(a^2 + l^2) \tag{3.5}$$

and for the cylinder;

$$I_{zz} = \frac{1}{2} mr^2 \tag{3.6}$$

If the width of the rectangular parallelepiped is much smaller than the length, $a \ll l$ as in the case of the two beams, then expression 3.6 can be rewritten as;

$$I_{xx} = \frac{1}{12} ml^2 \tag{3.7}$$

These expressions used in conjunction with Steiner's Theorem, results in the inertia for each part;

$$I_a = \frac{1}{12} m_a r^2 \tag{3.8}$$

$$I_b = \frac{1}{12} m_b l_b^2 + \frac{1}{2} m_b d_1^2 \tag{3.9}$$

$$I_c = \frac{1}{12} m_c l_c^2 \sin^2 \alpha + \frac{1}{2} m_c d_1^2 \tag{3.10}$$

$$I_d = \frac{1}{12} m_d \left(a^2 + l_d^2\right) + m_d d_2^2 \tag{3.11}$$

It should be noted that the vertical position of the load has no effect on the inertia, hence its placement is arbitrary. The inertia of the load is modeled as a box, the reason for this is that any arbitrary geometric shape that can fit into the box, has the same, or smaller, inertia. The torque required to rotate the crane is then;

$$\tau = (I_a + I_b + I_c + I_d)\dot{\omega} \tag{3.12}$$

3.2 Transmission

Choice of transmission type is governed by the amount of space available. For close range transmissions, or transmissions clogged in a small space, gear-type solutions are preferred in the shape of gearboxes. These allow moments and velocities to be scaled according to expression 3.13 below, where U is the gear ratio which decides the scaling.

$$\omega_1 = U\omega_2 \tag{3.13}$$

If there are no energy losses between the gears, expression 3.13 can be used to describe the transmission of torque, in this case the angular velocity is exchanged for torque in the expression above.

Another type of transmission is a belt or chain type, these are often used when there is a large distance between the two elements whom are considered. For these types, the "gear ratio" is given by the radius of the pulley which the belt or chain is wound around, resulting in the following expression;

$$r_2 = Ur_1 \tag{3.14}$$

Notice that expression 3.14 can be seen as an inversed version of 3.13 with angular velocity replaced by pulley radius.

When regarding belt transmissions, it is important to apply a pre-tension force, which ensures that the belt will not slip off from the pully during operation. This is done by either pushing the two pulleys away from each other after the belt has been attached, creating tension in the belt due to the deformation. Or by placing a roller between the pulleys, which pushes the belt. The belt is assumed to glide over the roller with almost no friction, thus resulting in no losses. The theory introduced here is taken from Vedmar [12], where further details about transmission mechanics can be found.

3.2.1 **Calculations on belt transmission**

As mentioned previously, calculations done on belt transmissions are limited to the calculation of the pre-tension force, which has to be applied. These calculations are close related to the dimensions and material aspects of the belt itself. The best way to dimension a belt is by looking at readily available products, which usually offer data and instructions on how to dimension the belt. In this case, products from the company Aratron are used, hence the following calculations and formulas are derived from their product catalogue [13].

There are several applications factors which appear in the formulas that need to be calculated before any further proceedings are made. These factors are related to the

type of load, motor used, operation time and gear ratio. However, not all of them are used and some are only applicable to specific belt types offered in the product catalogue. The belt type that will be used here is SYNCHROFLEX GENIII which only uses two application factors, load factor c_2 and step-up factor c_3. Values are chosen from tables in the catalogue and the total application factor is the sum of the two components;

$$c_0 = c_2 + c_3 \tag{3.15}$$

The application factor is then used as a multiplier in the calculations of tangential force, F_T, given by;

$$F_T = \frac{1.91 \cdot 10^7 \cdot c_0 \cdot P}{n_1 \cdot d_{k1}} \tag{3.16}$$

if the applied power *P* is known, expressed in kW. Or if the torque *M* is known, expressed in Nm, expression 3.16 becomes;

$$F_T = \frac{2000 \cdot c_0 \cdot M}{d_{k1}} \tag{3.17}$$

Here n_1 is the rotational speed, revolutions per minute (rpm), and d_{k1} the outer diameter in mm, both which are considered for the smaller pulley. The tangential force is the same as the normal force, hence the required pretension force can be calculated according to the guidelines given in the product catalogue, which are shown in table 1 below.

Table 1. Guidelines for pre-tension force calculations

Drive configuration	Pre-tension force
Two-pulley drive $\boldsymbol{Z_B < 60}$	$F_{pt} = 1/3 \cdot F_T$
Two-pulley drive $\boldsymbol{60 < Z_B < 150}$	$F_{pt} = 1/2 \cdot F_T$
Two-pulley drive $\boldsymbol{Z_B > 150}$	$F_{pt} = 2/3 \cdot F_T$

Z_B is the number of belt teeth and F_{pt} is the pre-tension force. The number of teeth on the belt is also tabulated data, but to find that out the belt length and width must be calculated according to;

$$L_b = \frac{\pi}{2} \cdot (d_{02} + d_{01}) + 2a + \frac{(d_{02} - d_{01})^2}{4a} \tag{3.18}$$

for the belt length and;

$$b = \frac{10 \cdot F_T}{Z_e \cdot F_{T/Z}} \tag{3.19}$$

for the belt width. Where d_{01} and d_{02} are the pitch circle diameter related to the small and large pulley respectively, expressed in mm. The distance between the pulleys is labeled as a, also measured in mm and $F_{T/Z}$ is the force transmittable by each tooth, read from specific product graphs as a function of rpm. The variable Z_e describes the number of teeth in mesh and is calculated as;

$$Z_e = \frac{Z_1}{2} - \frac{t \cdot Z_1}{2\pi^2 a}(Z_2 - Z_1) \tag{3.20}$$

The variables Z_1 and Z_2 represent the number of teeth for the small and large pulley respectively, where t is the pitch in mm. For each belt type, there is a maximum number of teeth that can be in mesh, shown in table 2 below, the result from 3.20 cannot exceed this number and is chosen instead.

Table 2. Limit on the number of teeth in mesh for different belt types.

Belt type	Max. number of teeth in mesh
CONTI SYNCHROCHAIN/FORCE	6 teeth
BRECOFLES and SYNCHROFLEX	12 teeth
SYNCHROFLEX GENIII	16 teeth

Using basic knowledge from solid mechanics and the behaviour of materials during deformation, the pre-tension force can be achieved by pulling the belt a distance δ given by;

$$\delta = \frac{F_{pt} L_b}{EA} \tag{3.21}$$

where E is the Young's Modulus and A the cross-sectional area of the belt. This expression and a reasonable value for E are given by Vedmar [12], in the chapter considering belt transmissions.

3.3 Bearings

To acquire a smooth motion, with minimal friction, between the moving parts, some sort of bearings are required. These are chosen from the SKF product catalogue [14], as the most common type of bearings, namely roller-bearings. Appropriate calculations used in the decision making are also introduced in the product catalogue.

The part in consideration, is the axis which connects the two beams. Since this part does not do complete revolutions and is limited to small motions, static conditions are applied. The equivalent static load bearing factor P_0 is calculated as;

$$P_0 = 0.6F_r + 0.5F_a \tag{3.22}$$

where F_r is the force in the radial direction and F_a in the axial direction. Furthermore, the following condition is applied;

$$P_0 < F_r \rightarrow P_0 = F_r \tag{3.23}$$

However, P_0 is not tabulated for different bearing types but instead the basic static load rating C_0 is shown. These two are related through the expression below.

$$C_0 = s_0 P_0 \tag{3.24}$$

s_0 is the safety factor, chosen as $s_0 = 2$ in this case.

It should be noted that the equations mentioned in this section are related to roller-bearings only and the reader is redirected to the SKF product catalogue [14] for any other type of bearing available. Roller bearings are chosen due to their low price and being a standard in the SKF collection.

3.4 Solid Mechanics

Three types of methods are used to solve the structural problems related to the development of the crane. As mentioned previously these are divided into an analytical problem, a semi-analytical problem and a numerical problem solved by using computer software. The fillet weld is also considered in this chapter and the stresses which occur at the weld when a load is applied to the beam.

3.4.1 **Analytical**

The analytical part is based on classic solid mechanics theories, there is a lot of literature which covers this topic, i.e. Ljung et al. [15] which will be used throughout this chapter. The methods applied here are related to the Euler-Bernoulli beam theory and the calculations of deformations and stress inside the beam.

By cutting the beam and creating a free-body diagram for each cut, the forces acting inside the beam can be calculated. These calculations are performed in the 2-D plane where the normal force has its positive direction to the right, the shear force upward and moments are positive in the clockwise (cw) direction. In this case, only stress in the normal direction is considered, since shear stress is too small and neglected.

$$\sigma_{xx} = \frac{N}{A} + \frac{M_b}{W_b} \tag{3.25}$$

Here, σ_{xx} is the normal stress, N the normal force, A the cross-section area, M_b the bending moment and W_b the section modulus. If the maximum stress is desired, then the maximum bending moment must be found. This is done by obtaining an expression of the bending moment as a function of the position, x, on the beam where the cut is placed. According to beam theory, the normal force is constant throughout a beam with a non-varying cross-section.

Another important tool used in classic beam theory are the elementary cases from which deformations can be calculated. These include five different loading cases applied for cantilever beams and simply supported beams. The elementary cases are derived by expressing linear deformation as a function of position, $w(x)$. By

differentiating this function with respect to x, angular deformation, forces and moments can be derived and thus all components are expressed with the same variable. Integration and application of boundary conditions results in a complete expression which describes the deformation for any point on the beam.

These cases are only capable of describing the deformation for specific loading situations, however any arbitral state can be described as a superposition of the elementary cases, hence they prove to be very useful when dealing with statically indeterminant problems.

This analysis is done on the axis and horizontal beam, which are the components who carry the load. The load is applied to the horizontal beam, and thus it is logical to begin the analysis on this part, even if it belongs to phase 2 and is designed after phase 1. Figure 3 below shows the free-body diagram of a possible design, where the part has been cut at the intersection between two beams and by the wall. The load is modelled as a point force acting at the end.

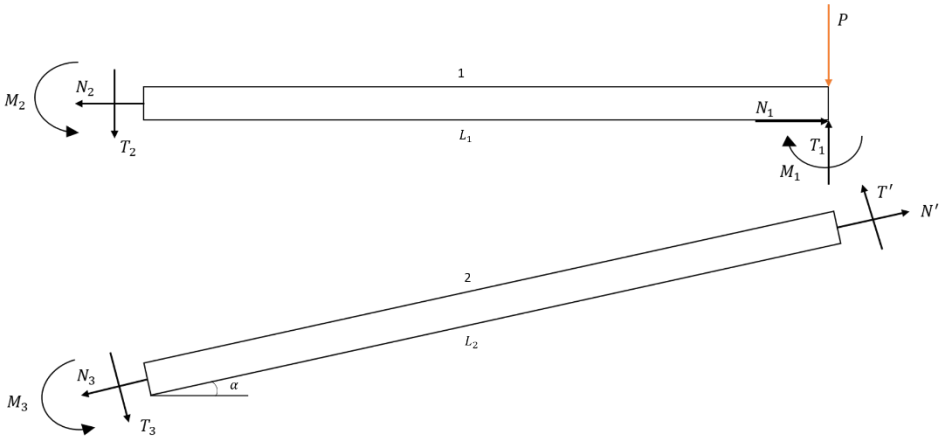

Figure 3. Free-body diagram of the horizontal beams on the crane, applied load is shown as a red arrow and reaction forces as black. The beams are labeled as 1 and 2.

The free-body diagram from figure 3 yields the following equilibrium equations;

$$(\uparrow): T_1 - T_2 - P = 0 \tag{3.26}$$

$$(\rightarrow): N_1 - N_2 = 0 \tag{3.27}$$

$$(\curvearrowleft): M_2 - M_1 - PL_1 + T_1 L_1 = 0 \tag{3.28}$$

for beam 1 and

$$(\uparrow): T' - T_3 = 0 \tag{3.29}$$

$$(\rightarrow): N' - N_3 = 0 \tag{3.30}$$

$$(\curvearrowleft): M_3 - M_1 - T'L_2 = 0 \tag{3.31}$$

for beam 2. The primed forces, N' and T' are related to N_1 and T_1 as;

$$N' = T_1 \cos\alpha + N_1 \sin\alpha \tag{3.32}$$

$$T' = T_1 \sin\alpha - N_1 \cos\alpha \tag{3.33}$$

The lengths are related according to;

$$L_1 = L_2 \cos\alpha \tag{3.34}$$

This problem is statically indeterminant, therefor deformations constraints have to be applied if this problem is to be solved. There are nine unknowns and six equations, hence three deformation equations are required. The beams can be modelled as cantilever beams, but on a closer look it will be better to approximate them as simply supported beams, since they support each other at the end. To better match their cantilever characteristics, the angle at the wall support is set to zero for both beams. Elementary case 5 for simply supported beams from Ljung et al. [15] agrees the most with the current discussion and is used for these beams. However, the end-point deformation of the complete structure will still resemble more a cantilever than a simply supported beam, since the later has no linear deformation at the end. This is accounted for by superimposing elementary case 1, for cantilever beams. Figure 4 shows the deformation and elementary cases used to approximate the problem above.

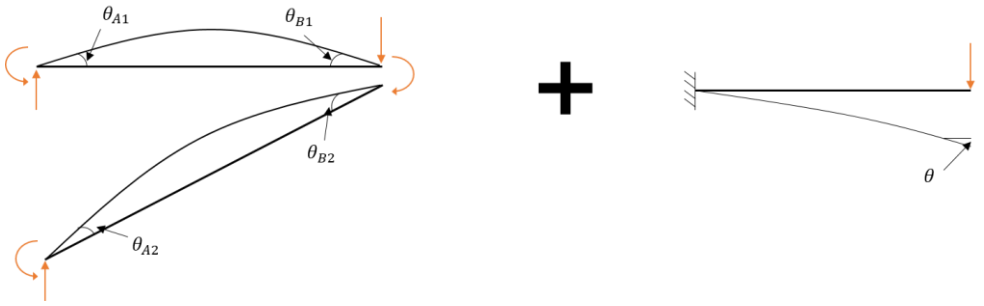

Figure 4. Deformation conditions for the beams as a combination of two elementary cases.

Considering the direction of the angular deformation in figure 4, it can be seen that the direction of θ is opposite that of θ_{B1} and θ_{B2}. It can also be noted that in this case the angular deformation at the endpoint is very small, almost zero. Furthermore, both beam 1 and 2 will deform the same around their common endpoint, thus $\theta_{B1} = \theta_{B2}$. Using notations taken from figure 4, the deformation conditions are;

$$\theta_{A1} = \theta_{A2} = 0 \tag{3.35}$$

$$\theta_{B1} = \theta_{B2} \tag{3.36}$$

$$\theta_{B1} + \theta_{B2} - \theta \approx 0 \tag{3.37}$$

From elementary case 5 for simply supported beams, the angles are defined as;

$$\theta_{A1} = \frac{M_2 L_2}{3EI}\cos\alpha + \frac{M_1 L_2}{6EI}\cos\alpha \tag{3.38}$$

$$\theta_{A2} = \frac{M_3 L_2}{3EI} + \frac{M_1 L_2}{6EI} \tag{3.39}$$

$$\theta_{B1} = \frac{M_2 L_2}{6EI}\cos\alpha + \frac{M_1 L_2}{3EI}\cos\alpha \tag{3.40}$$

$$\theta_{B2} = \frac{M_3 L_2}{6EI} + \frac{M_1 L_2}{3EI} \tag{3.41}$$

and from elementary case 1 regarding cantilevers, the angle is defined as;

$$\theta = \frac{PL_1^2}{2EI} \tag{3.42}$$

In these equations, E is the Young's modulus of the material and I the inertia around the bending axis. The linear deformation at the end-point of the beam is;

$$\delta = \frac{FL_1^3}{3EI} \tag{3.43}$$

In this case, F is the difference between the load P and the force T_1 which is opposite in direction from P and works to pull up the structure.

The system in figure 3 can now be solved by using the equilibrium equations 3.26-3.31 together with the deformation constraints 3.35-3.37. When this is done, the stress in the axis can be calculated. The procedure is similar as before, a free-body diagram of the axis is drawn, shown in figure 5. Because there are bearings attached to the ends of the axis, the endpoints are tightly secured and result in a moment. But according to Vedmar et al. [16], bearing supports result in no moments, thus this becomes a special case when the reaction moments are ignored. However, there will still be a bending moment in the axis which must be accounted for during stress calculation. Moreover, only the upper bearing allows movement in the vertical direction, consequently there is no vertical reaction force present there.

From figure 5, the equilibrium equations for the axis are;

$$(\uparrow): N_2 + N' + H_A + H_B = 0 \tag{3.44}$$

$$(\rightarrow): V_B - T_2 - T' + mg = 0 \tag{3.45}$$

$$(\curvearrowleft): M_2 + M_3 - N_2\left(\beta - \frac{\alpha}{2}\right)L - H_A\beta L + T_2 2r + T' 2r - mgr = 0 \tag{3.46}$$

Here the reaction forces are labeled as H_A, H_B and V_B. The axis is actually vertical but is displayed in a horizontal state in the figure, hence the reason why the direction

of the gravitational force is pointing towards the right instead of down, which is the intuitive way. Additionally, the external forces and moments are taken from the free-body diagram in figure 3, where the same notations have been kept. The scale factors α and β are used in the equations related to the elementary cases. Notice that for N', α becomes β, since $\alpha = 1 - \beta$ and vice versa.

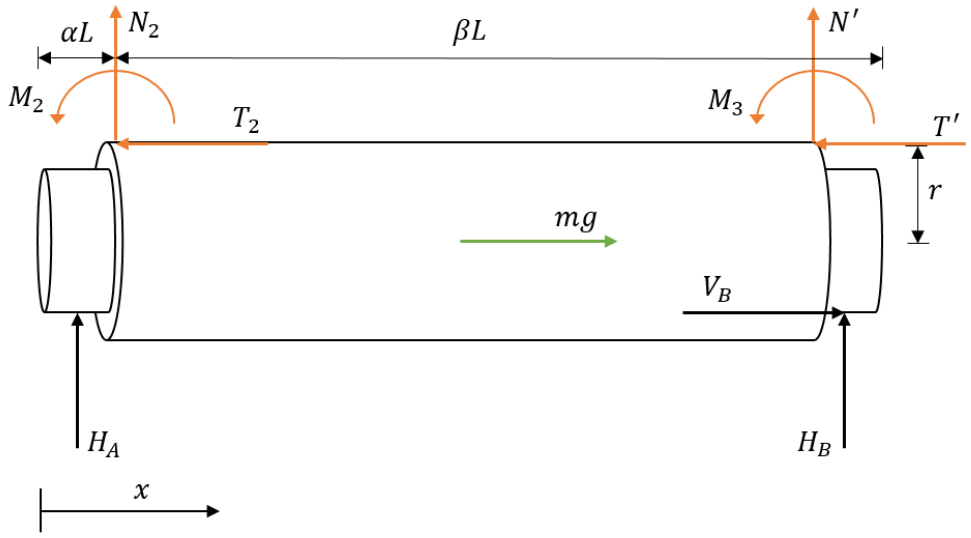

Figure 5. Free-body diagram of the axis from phase 1, with reaction forces from bearings drawn as black arrows. The load is taken from the beams connecting to the axis.

The system in figure 5 can be solved using only the equilibrium equations, 3.44-3.46. But since the stress calculations require knowledge about the maximum bending moment in the axis, the axis must be cut and the moment calculated. For this situation, the maximum bending moment might occur at any of the positions where the load is applied, therefore the axis is cut at these points. The two cuts are shown in figures 6 and 7, for the left end and right end cut respectively.

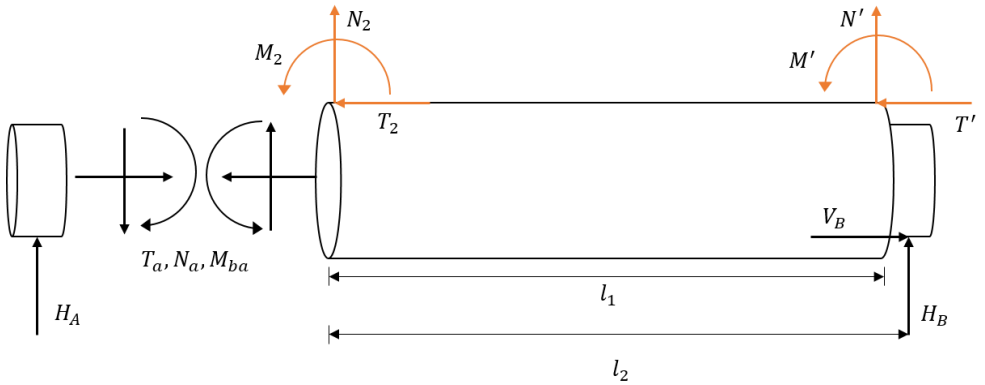

Figure 6. Free-body diagram of the left-end cut in the axis. Inner forces and moments are labeled as T_a, N_a and M_{ba}.

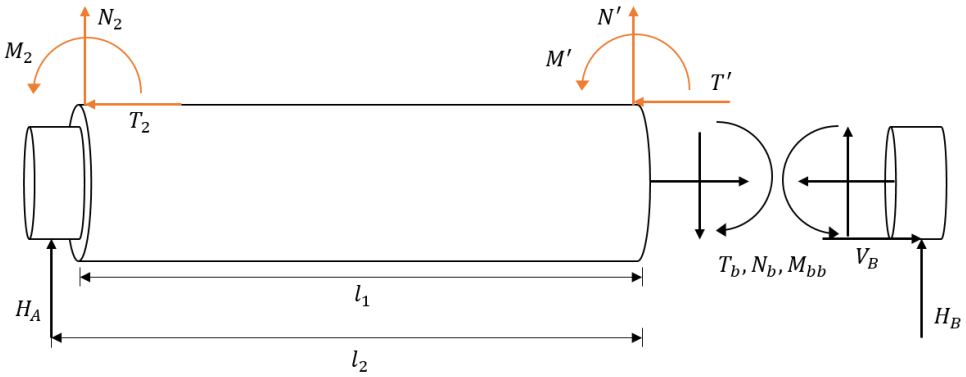

Figure 7. Free-body diagram of the right-end cut in the axis. Inner reaction forces and moments are labeled as T_b, N_b and M_{bb}.

Starting with figure 6, and only considering the cylinder, moment equilibrium around the point where the cut is placed gives;

$$(\curvearrowleft): M_2 + M' + M_{ba} + H_B l_2 + N' l_1 = 0 \tag{3.47}$$

Similarly, for the right-side cut in figure 7;

$$(\curvearrowleft): M_2 + M' - M_{bb} - H_A l_2 - N_2 l_1 = 0 \tag{3.48}$$

Solving equations 3.47 and 3.48 for the bending moments result in;

$$M_{ba} = -M_2 - M' - H_B l_2 - N' l_1 \tag{3.49}$$

$$M_{bb} = M_2 + M' - H_1 l_2 - N_2 l_1 \tag{3.50}$$

Using these equations, the reaction moments and forces are calculated and thus the maximum bending moment can be found. This moment, together with the vertical resultant of the force, is inserted in equation 3.25 to yield the maximum stress in the axis. However, stress concentrations are not accounted for in the current calculations. In order to do so, a shape factor K_t is introduced, which is a multiplier applied to the maximum stress. Consider a shape where the cross-section diameter changes from d to a larger diameter D, while the corner radius is ρ. Then the shape factor K_t is a function of ρ/d and D/d, which is plotted in a diagram for different sizes. This diagram can be found in Ottosen et al. [17], or in any good solid mechanics handbook. The maximum stress in an axis with different cross-section diameter is then calculated as;

$$\sigma_{tot} = K_t \cdot \sigma_{max} \tag{3.51}$$

where σ_{max} is the maximum stress calculated previously, using equation 3.25. When using this method, the smallest cross-section diameter should be considered for 3.25 and then adjusted as described in 3.51.

The deformation of the axis is calculated a bit differently than for the beam, since the load conditions are different. If the deformation is exaggerated, the axis will form an S-shape, thus the maximum deformation occurs at a point, $1/4L$ from the end. Even though the part in question is an axis, it can be modelled as a beam and thus the elementary cases for beams can be applied. This system is modelled as a combination of two simply supported beams, namely case 1, and 2 from Ljung et. al. [15], where the contribution of the horizontal forces is considered in case 1 and the moments in case 2. The linear deformation can then be calculated as a sum of the deformations for each elementary case.

$$\delta_{11} = \frac{N_2 L^3}{6EI}\beta((1-\beta^2)\xi - \xi^3) \tag{3.52}$$

$$\delta_{12} = \frac{N' L^3}{6EI}\alpha((1-\alpha^2)\xi - \xi^3) \tag{3.53}$$

$$\delta_{21} = \frac{M_2 L^2}{6EI}((1-3\beta^2)\xi - \xi^3) \tag{3.54}$$

$$\delta_{22} = \frac{M_3 L^2}{6EI}((1-3\alpha^2)\xi - \xi^3) \tag{3.55}$$

Equations 3.52-3.55 show the deformations at a point located a distance ξL from the edge of the axis, for elementary case 1 and 2 respectively. When summing the deformations, it is important to keep in mind the directions and to assign a positive direction. In this case, the positive direction is taken pointing up in figure 5. Thus, the total deformation becomes:

$$\delta = -\delta_{11} - \delta_{12} + \delta_{21} + \delta_{22} \tag{3.56}$$

3.4.2 **Semi-analytical**

The semi-analytical solution is done by using CALFEM to calculate the reaction forces and deformations, then equation 3.25, which was mentioned in the previous section, is used to calculate the stress. CALFEM is a MATLAB based FEM program, which is founded on the theory of virtual work, discussed in Ottosen et al. [17]. Detailed descriptions and examples of functions available in CALFEM can be found in the manual [10].

To conduct an analysis, a mesh is created and stored in a matrix element in MATLAB. The important values are the degrees of freedom and coordinates of the nodes in the mesh. Then a stiffness matrix can be created which relates the material properties to each element in the mesh. The global stiffness matrix, $\boldsymbol{K}$, is related to the displacement vector, $\boldsymbol{u}$, and load vector, $\boldsymbol{f}$, according to;

$$\boldsymbol{f} = \boldsymbol{K}\boldsymbol{u} \tag{3.57}$$

The biggest advantage with using CALFEM is that the forces are calculated for each DOF, at each node in the mesh. Thus, a point force can easily be obtained and inserted in the formulas derived from a free-body diagram. It is however important to notice that beams require three DOF at each node, while bars only need two, since bars do not transfer moments.

3.4.3 **Numerical**

In this case the numerical method refers to FEM calculations done using ANSYS. These methods are similar to the ones done in CALFEM, the big difference being that the mesh is automatically generated in the program and that the results is obtained as a colourful chart. Point forces are difficult to obtain, same goes for modelling point loads, since they are distributed over a surface. However, a finer mesh can be obtained more easily, since the program automatically generates it, all that needs to be defined are element sizes and where to place the mesh.

The FEM analysis done in ANSYS requires a CAD-file as an input geometry. A user defined mesh is applied on this geometry along with boundary conditions and loads. The principles are the same as for any FEM program which are based on the principle of virtual work and the relation described in 3.57. Virtual work will not be described in depth here, nor will the theory behind FEM, but the reader is redirected to Ottosen et al. [17;18].

FEM calculations which use a fine mesh are generally good at picking up stress concentrations, since the mesh covers all surfaces of the 3D geometry. Therefore, there is no need for additional work if stress concentrations are to be considered in the calculations.

3.4.4 **Weld stress**

The weld is usually the weakest part in the structure, due to the impurities which are formed in the material during welding [19]. In order to avoid catastrophic failure or accidents involving the structure, it is important to calculate the maximal stress which occurs in the weld. This can be a tedious task and there are many theories on how to obtain the most correct result. In this study, the calculations are done according to [19] and using European norms (EN) [20]. It is assumed that only fillet welds are used.

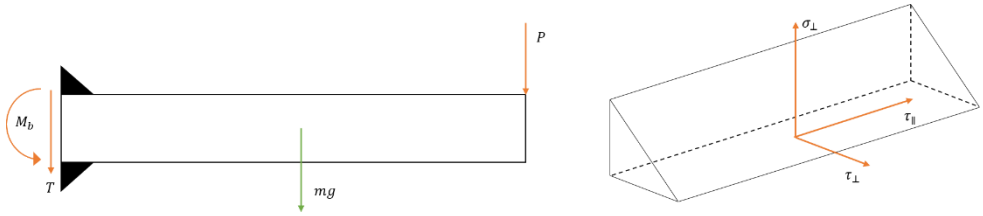

Figure 8. Horizontal beam welded to a vertical material. The beam is shown to the left in the figure, with the load P acting on the end and reaction moment and shear force from the wall. Detailed description of the weld is shown to the right with the direction of stress in the weld. The size of the weld is exagerated for demonstrational purpose.

An example of a beam welded to a wall is shown in figure 8. The weld is placed on the top and bottom face of the beam, applied only on a single side. A force P is applied at the end of the beam which gives rise to stresses in the weld acting in three different directions, a normal stress and two shear stresses. The normal stress acts perpendicular to the bottom plane, seen in figure 8 and labelled as $\sigma_\perp$. The two shear stresses are labelled as $\tau_\perp$, which is perpendicular to the plane and $\tau_\parallel$, which acts in the parallel direction of the plane.

The applied force and self-weight of the structure directly influence the perpendicular shear stress, calculated using the relation between force and stress, derived in basic solid mechanics, see Ljung et al. [15].

$$\tau_\perp = \frac{P+mg}{A_w} \tag{3.58}$$

Here A_w is the area of the fillet weld on the beam. It is important to use the effective length of the weld which is described as;

$$l_w = l - 2a \tag{3.59}$$

where l is the total length of the weld and a is the weld throat thickness. The weld throat thickness is chosen by the designer and may not exceed the thickness of the material welded together.

A bending moment will result at the wall as a reaction from applied force and self-weight. This moment gives rise to a stress in the normal direction, something which has been discussed in the previous section. The stress is calculated by applying equation 3.25 to the current situation, resulting in;

$$\sigma_\perp = \frac{M_b}{I_w} z \tag{3.60}$$

where M_b is the bending moment, I_w the moment of inertia for the weld and z the distance from the centre-line to the top of the beam. The inertia might be difficult to derive and formulas for several types of welds are available from MITCalc [18]. It might be noticed that there is no parallel shear stress $\tau_\parallel$ in these calculatins, this is because there is no component which gives rise to a stress in that direction for the situation described in figure 8.

The total equivalent stress is obtained by using von Mises' theorem, defined in Ottosen et al. [17]. Applied to the weld, the theorem yields;

$$\sigma_m = \sqrt{\sigma_\perp^2 + 3(\tau_\perp^2 + \tau_\parallel^2)} \tag{3.61}$$

In order to make sure that the weld will hold, the total equivalent stress has to be less than the yield stress σ_y, for the material used in the electrode, divided by a correlation factor β and a partial safety factor γ_w. This is done according to Eurocode 3 [20], where the correlation factor changes depending on the type of electrode used.

$$\sigma_m < \frac{\sigma_y}{\beta\gamma_w} \tag{3.62}$$

4 Results

4.1 Design

4.1.1 **First phase**

The design of phase 1, seen from different views, is shown in figure 9 below. Starting from the top left and going clockwise, 9a shows the top view of the vertical beam. Here a motor is placed which will drive the axis and thus enable the rotating motion of the crane. Power is transmitted from the motor through a toothed belt which is connected to two pullies, who are fastened to the motor axis and crane axis. The motor is in turn secured with screws to a plate which has two guidelines cut out. These allow linear motion and thus position adjustment of the motor and plate, which is necessary when fitting the belt to the pullies. By moving the plate and motor, the required pre-tension force is achieved in the belt. Figure 9b shows the side view of the beam, where the motor can be seen more clearly hanging from the back and how the belt is placed on the pullies.

The plate is in turn fastened to the top of the beam by four screws which go into four threaded holes, and a fifth screw which is perpendicular to the previous ones. Position is adjusted by first moving the plate to a desired point, then the fours screws are inserted, and since the guidelines are thinner than the screw head, the contact forces between the heads and the plate will push the plate down. The fifth screw is used to secure the position of the plate from the side, preventing the pre-tension force to push the motor towards the axis.

Figure 9c shows a detailed view of where the bottom bearings are placed on the beam, this looks the same for both top and bottom bearings. The bottom bearing is completely fastened and does not allow for motion in any direction, while the top bearing can move in the axial direction. This is achieved by using the weight of the axis to push down the bottom bearing, the top bearing does not carry the axis and is thus allowed to slide in the axial direction. It is however noteworthy to mention that both holes are the same size since same type of bearings are used, more importantly they are large enough to let the axis fit through. This is important for the assembly process and will be discussed further in section 4.2.

The last part included in phase 1 is the axis, which is shown in figure 10. As seen from the figure, different diameters are used at different sections of the axis, the

reason for this is to fit the double bearings at each side and enable the bottom bearing to carry the axis. Two tracers have also been added which will be used when connecting the beam from phase 2 to the axis. The axis in figure 10 has been laid down horizontally, if figures 9 and 10 are compared, it can be noticed that the right part of the axis in figure 10 is the part which comes out of the top of the beam in figure 9a and 9b.

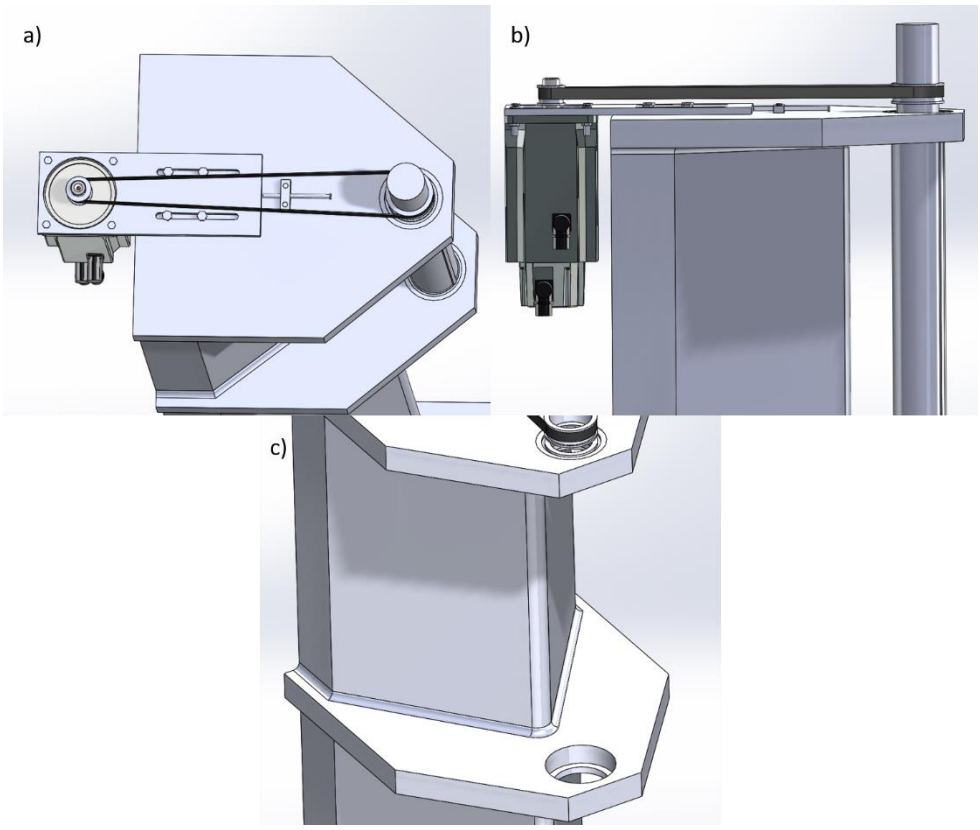

Figure 9. CAD model of the final design of the beam in phase 1. a) shows the top view of the beam while b) shows the side view. The hole in which the bottom bearing is placed, is shown in c).

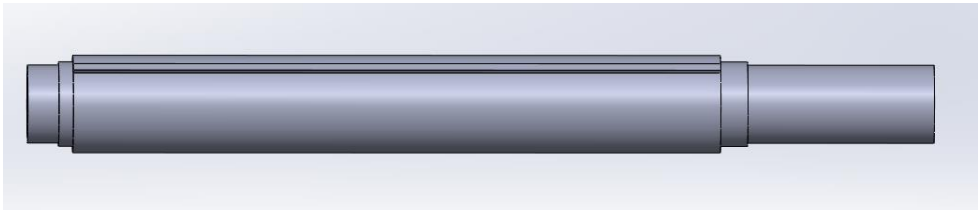

Figure 10. CAD model of the axis, laid down horizontally.

4.1.2 **Second phase**

Figure 11 shows the design of the second phase, the horizontal beam is first cut where one part is attached to a hollow cylinder. Supports are added to help carry the load and ease the amount of endpoint deformation. As mentioned previously, the horizontal beam is bough from Güdel [4] and is fitted with racks on which a robot can traverse. The racks are placed on the side of the beam, as seen in the figure, this is done to make the placement of the robot easier.

On the inside of the cylinder, two traces are cut in order to connect the current part with the axis from phase 1. The supports and the beam are both welded together, and in turn to the cylinder. Regarding the supports, they could be bought from a dealer in one of the standard dimensions, i.e. 30x60 mm square-cross-section pipe.

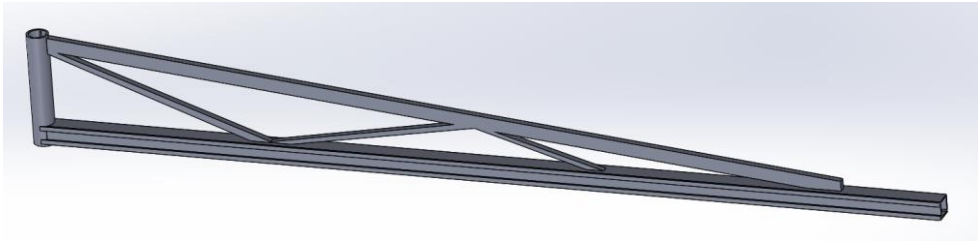

Figure 11. CAD model showing the design of the second phase, a Güdel beam attached to a hollow cylinder and fitted with supports.

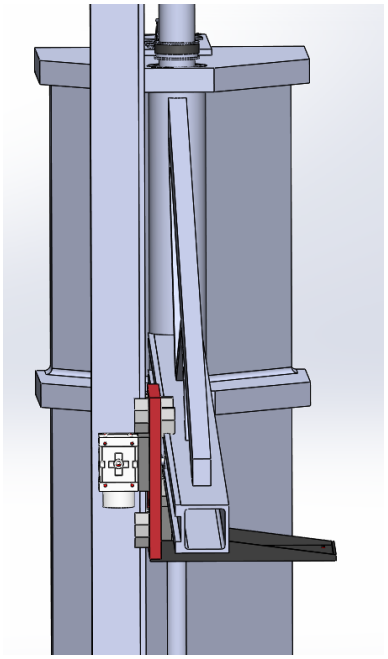

Figure 12. Front view of how the beams are assembled together with a robot which allows linear motion along the y- and z-axis.

The robot which will move along the side of the beam will have the other part of the cut beam attached to it, perpendicular with the one seen in figure 11. This second part will in turn be able to move up and down, what can be defined as linear motion along the z-axis. Figure 12 illustrates how this part is assembled, the robot is also bought from the same manufacturer and is fitted with two motors which connect to a pinion, the pinion is connected to the rack on the beam. By rotating the pinions, the beams are moved in either direction.

4.1.3 **Final assembly**

A CAD 3D model of the complete crane, when all parts have been assembled, is shown in figure 13. Note that the extruder has not been modelled and mounted on the crane, nor are the cables which connect the motors to their power supply modelled. The idea is to let the cables which connect to the robot, seen as the red and black "L" shape, run along the bottom part of the horizontal beam. When placed like this, they will not interfere with the motion of the robot. The motor at the back of the beam can easily be connected to a power supply without causing interference to any of the other parts.

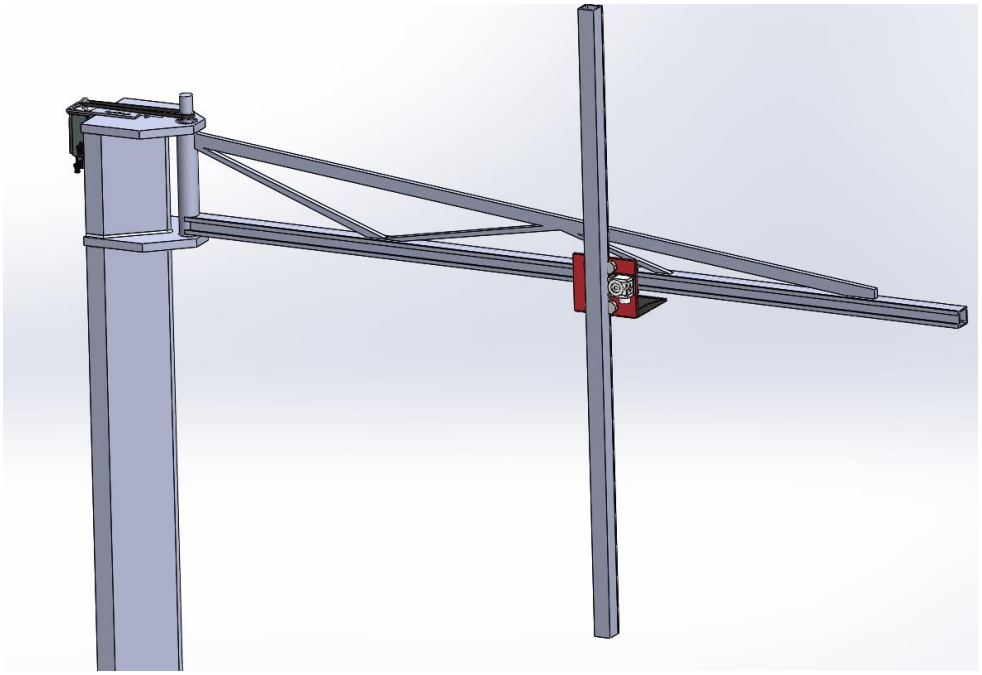

Figure 13. CAD model of the complete assembly of the crane. Extruder has not been mounted, nor are cables which power the motors seen.

4.2 Assembly

During the assembly special attention must be made to the connection between the two beams, vertical beam with axis, and horizontal beam which is welded to a hollow cylinder. This includes how and in which order to place the bearings, axis and phase 2 part, i.e. the cylinder with robot. First the bottom bearing is placed in the hole cut out in the vertical beam, shown in figure 9c. Then the phase 2 cylinder, is placed between the two plates on the vertical beam. The phase 2 part must be kept in place while the axis is threaded through the top of the beam, cylinder and finally into the bottom bearing. When this is complete, the top bearing is placed in the top hole and thus the assembly is complete. The other parts can then be put in place in any desired order. In this assembly the axis acts as a pin which keeps the cylinder together, connecting the horizontal beam to the motor on the top of the vertical beam.

The assembly is reversible, the crane can be disassembled and to do so, the axis which acts as a pin keeping the different parts together, should be removed first. This is achieved by using a mechanical extractor, which can be bought at any hardware store. The tool is attached to the bottom of the beam and centred under the axis. When wound, it pushes the axis upwards, allowing it to be pulled out from the top, which then releases the cylinder and beams. The bottom bearing can also be removed by using the same tool, just by pushing further after removing the cylinder.

4.3 Calculations

Calculations are done based on the theory derived previously in chapter 3. Hence there are several different types of calculations which must be conducted and all will be presented here, divided in different sub-sections. In some sub-sections, both analytical and semi-analytical results will be presented.

4.3.1 **Deformation**

Deformation calculations are done both analytically and semi-analytically, as mentioned in chapter 3. The deformation calculations are first done on the horizontal beams in phase 2, which will be done using equations 3.26-3.43. Furthermore, the crane is designed to carry a load of 125 kg at its endpoint, thus setting

$$P = 125 \cdot 9.81 \approx 1230\text{N} \tag{4.1}$$

Before the end-point deformation can be calculated, and the required equations solved, some material and shape properties of the beams must be introduced. These

are shown in table 3 below. Young's modulus E, is taken from tabulated data for steel and the inertia I, is calculated from tables using the cross-section dimensions of the beam found in [4]. The formulas and tabulated data are taken from Sundström et al. [21].

Table 3. Initial values required to solve the equilibrium and deformation equations of the beams in phase 2.

Parameter	Notation	Value
Beam 1 length	L_1	4m
Angle	α	7.125°
Young's Modulus	E	210GPa
Beam 1 inertia	I_1	$1.89 \cdot 10^{-6}\text{m}^4$
Beam 2 inertia	I_2	$1.08 \cdot 10^{-7}\text{m}^4$

Now the values from table 3 and the load from 4.1 are inserted in equations 3.26-3.43 to solve for the deformation of the beams in phase 2, which yields

$$\delta_{beam,a} = 0.0043\text{m} \tag{4.2}$$

This result is obtained by inserting the values in the analytical expressions derived previously. The semi-analytical result is obtained by using CALFEM. There are two ways in which the deformation can be obtained. It can either be calculated by extracting the inner force T_1, shown in figure 3, and inserting it in 3.43. Or the deformations at the nodes are directly calculated using 3.57. A node is placed at the end, and thus the deformation can be obtained using this method, the result is:

$$\delta_{beam,s} = 0.0033\text{m} \tag{4.3}$$

It should be mentioned that both semi-analytical methods yield the same result, namely the one shown in 4.3. Furthermore, the MATLAB code used for CALFEM is found in Appendix C where the same code is used for all calculations.

Table 4. Design values for the axis, required to solve the deformation equations. Shape factor and Young's modulus are found in Söderberg [21].

Parameter	Notation	Value
Axis length	L	0.53m
Distance cut and load	l_1	0.5m
Distance cut and support	l_2	0.515m
Alpha fraction	α	0.0283
Beta fraction	β	0.9717
Young's Modulus	E	210GPa
Axis inertia	I	$6.36 \cdot 10^{-7}\text{m}^4$
Xi fraction	ξ	0.25
Shape factor	K_t	2.8

The maximum linear deformation of the axis is obtained by calculating equations 3.52-3.55 and inserting in 3.56. Using the values shown in table 4, the following deformation is obtained from the analytically derived reaction forces;

$$\delta_{axis,a} = 2.0485 \cdot 10^{-4}\text{m} \approx 0.2\text{mm} \tag{4.4}$$

Inserting the reactions forces obtained through CALFEM in equations 3.52-3.55 and further into 3.56 results in the following deformation;

$$\delta_{axis,s} = 5.7042 \cdot 10^{-5}\text{m} \approx 0.06\text{mm} \tag{4.5}$$

No mesh was created for the axis; therefore, the same analytical expressions are used in the calculation, the difference being how the reaction forces are obtained.

4.3.2 **Stress**

After equations 3.26-3.43 have been solved, the maximum stress in the beam can be calculated using 3.25. The normal force is constant throughout the beam; therefore, the choice is arbitrary. However, the maximum bending moment must be found, which occurs at either end of the beam. Comparing the moments yields the following results;

$$M_1 < M_2 = 2.462\text{kNm} \tag{4.6}$$

$$M_1 < M_3 = 2.519\text{kNm} \tag{4.7}$$

for the horizontal and diagonal beam respectively, seen in figure 3. Inserting the normal forces, N_2 for the horizontal beam and N' for the diagonal, in 3.25 together with the moments from 4.6 and 4.7, gives;

$$\sigma_{beam,1a} = 52.32\text{MPa} \tag{4.8}$$

$$\sigma_{beam,2a} = 35.15\text{MPa} \tag{4.9}$$

for the horizontal and diagonal beam respectively.

Semi-analytical results are obtained in a similar way, by inserting the reaction forces and moments in equation 3.25. Maximum bending moment occurs at the wall support, as previously concluded, and inserting values in 3.25 yields;

$$\sigma_{beam,1s} = 13.13\text{MPa} \tag{4.10}$$

$$\sigma_{beam,2s} = 8.57\text{MPa} \tag{4.11}$$

Maximum stress in the axis is calculated by inserting the maximum bending momentum and resultant normal force in 3.25. Then 3.51 is used to adjust for the stress concentrations which occur in the axis. The maximum bending moment is found by comparing equations 3.49 and 3.50 to each other. Inserting values obtained from the equilibrium equations 3.44-3.46 for the axis, in 3.49 and 3.50, results in the following:

$$M_{ba} = M_{bb} \tag{4.12}$$

Thus, it becomes arbitrary which moment to choose, since they are both equal. Inserting the forces and moments, obtained by analytical methods, and which act on the axis in 3.25 gives;

$$\sigma_{axis,a} = 6.089\text{MPa} \tag{4.13}$$

and further insertion in 3.51 with the shape factor taken from table 4 gives:

$$\sigma_{axis,tota} = 17.05\text{MPa} \tag{4.14}$$

Using the reactions obtained by CALFEM instead, gives the following results:

$$\sigma_{axis,s} = 5.549\text{MPa} \tag{4.15}$$

$$\sigma_{axis,tots} = 15.54\text{MPa} \tag{4.16}$$

Lastly the stress in the weld is calculated and for these calculations only the larger beam is considered, i.e. the Güdel ZP-I beam. The assumption is made that if the weld can sustain the larger beam, it should also be enough for the smaller, since the same weld throat thickness a is used. Table 5 shows the values used in the calculations.

Table 5. Values used in the weld stress calculations. The partial factor and correlation factor are obtained from tabulated data in Eurocode 3[19].

Parameter	Notation	Value
Weld throat thickness	a	0.005m
Effective weld length	l_w	0.070m
Weld area	A_w	0.0014mm^2
Weld moment of inertia	I_w	$1.272 \cdot 10^{-6}\text{m}^4$
Partial factor	γ_w	1.25
Correlation factor	β	0.8
Mass of the beam	m	68.8kg

The effective weld length is calculated using equation 3.59, while the area and inertia are obtained from formulas, provided by MITCalc [19]. Weld throat thickness is decided in the design while the partial and correlation factor are obtained in Eurocode 3 [20]. The mass of the beam is obtained from Güdel [4].

Inserting the values from table 5 in equations 3.58, 3.60 and 3.61 gives the following result;

$$\sigma_{weld} = 171.17\text{MPa} \tag{4.17}$$

If an electrode with the yield stress $\sigma_y = 235\,\text{MPa}$ is used then relation 3.62 becomes;

$$\sigma_{weld} = 171.17\text{MPa} < 235\text{MPa} \quad (4.18)$$

and the conditions is satisfied.

4.3.3 **Bearings**

The equivalent static load bearing factor P_0, shown in 3.22 is calculated by identifying the axial and radial forces and inserting them into the equation. Calculations are done on the axis, and the forces are identified using figure 5.

$$F_r = H_B = 10.16\text{kN} \quad (4.19)$$

$$F_a = V_B = 1.396\text{kN} \quad (4.20)$$

These values are obtained from CALFEM using the equilibrium equations for the axis, 3.44-3.46, to obtain the reaction forces. The static load bearing factor can then be calculated using 3.22;

$$P_0 = 6.797\text{kN} \quad (4.21)$$

It can clearly be seen when comparing 4.21 to 4.19 that $P_0 < F_r$, therefor the condition in 3.23 states that:

$$P_0 = F_r = 10.16\text{kN} \quad (4.22)$$

The basic static loading is calculated by inserting 4.22 in 3.24 with the safety factor $s_0 = 2$;

$$C_0 = 20.33\text{kN} \quad (4.23)$$

If the same process is repeated but instead of using the reaction forces obtained through CALFEM, use the reaction forces obtained by analytical results in 4.19 and 4.20. The basic static loading coefficient becomes;

$$C_0 = 14.45\text{kN} \quad (4.24)$$

According to SKF [14] there is one bearing which has an inner diameter of $d = 60\,\text{mm}$, outer diameter $D = 95\,\text{mm}$ and basic static loading coefficient $C_0 = 23.2\text{kN}$. The bearing in question has the ID 6012 in the SKF catalogue. However, this will not be enough, in order to ensure that a heavy load can be applied, an additional bearing will be used. The bearing is inserted at the larger diameter, therefor a bearing with $d = 65\text{mm}$ needs to be found. Bearing with ID 16013, fulfils this requirement, the outer diameter is $D = 100\,\text{mm}$ and basic static loading coefficient $C_0 = 19.6\text{kN}$. The total thickness of the two bearings combined is $b = 29\text{mm}$. The total static loading coefficient is the sum of the two;

$$C_0 = 19.6 + 23.2 = 42.8\text{kN} \tag{4.25}$$

These two bearings create a set, and two of these sets will be used in support of the axis, one at the bottom and one at the top. The set is inserted in the hole, seen figure 9c, and fitted to the axis through the different cross-section diameters. Therefore, one type of bearing is fitted to a certain diameter.

4.3.4 **Transmission**

For the power transmission, a toothed belt will be used of type SYNCHROFLEX AT3 GENIII, ordered from Aratron [13]. The power will be transmitted from a motor of type QSY 130 C EcoDyn, specifications about the motor are available at the manufacturer's website [22]. From the specifications sheet, the diameter of the motors axis is $d_m = 24$mm. It is already known from the design that the diameter of the crane axis is $d_a = 60$mm, two pullies matching these specifications are found accordingly. But before the calculations can be done, the application factors c_2 and c_3 must be decided, tabulated data for these factors is found in the product catalogue [13].

The load factor c_2 is decided based on the motor size and mass to be accelerated. In this case a small motor is used to accelerate a large mass, which results in a load factor of $c_2 = 2.8$. The step-up factor c_3 depends on the size of step-up used in the transmissions and since the power is transmitted from a smaller pulley to a larger, there is no step-up, i.e. $U < 1$ in 3.14. Values which will be used in the calculations are summarized in table 6 below.

Table 6. Values used in the transmission calculations. Centre distance is obtained from the design, motor values from Heidenhain [22] and the remaining values are taken from Aratron [13].

Parameter	Notation	Value
Centre distance	a	520mm
Motor rated power	P_h	1.6kW
Motor rated torque	τ	5.2Nm
Motor rated speed	n	3000rpm
Small pulley teeth	z_1	36
Large pulley teeth	z_2	74
Small pulley diameter	d_{k1}	33.97mm
Large pulley diameter	d_{k2}	70.25mm
Pitch	t	3mm
Pitch circle diameter small	$d_{01} = z_1 t/\pi$	34.38mm
Pitch circle diameter large	$d_{02} = z_2 t/\pi$	70.66mm
Load factor	c_2	2.8
Step-up factor	c_3	0

Inserting the load- and step-up factor in 3.15 gives the following application factor;

$$c_0 = 2.8 \tag{4.26}$$

Inserting torque, diameter of the small pulley and 4.26 in 3.17;

$$F_{T\tau} = 673.54\text{N} \tag{4.27}$$

If instead 3.16 is used, where the rated power from the motor is inserted together with the rated speed, the result becomes:

$$F_{TP} = 659.71\text{N} \tag{4.28}$$

The total length of the belt is calculated using 3.18, putting in the correct values from table 6 yields the following result:

$$L_b = 1206\text{mm} \tag{4.29}$$

From the curve plotted for ATG3 GENIII in the product catalogue [13], the tangential force transmitted by a tooth in mesh is:

$$F_{T/Z} = 25\text{N}/10\text{mm} \tag{4.30}$$

The number of teeth in mesh is calculated by using the values from table 6 in 3.20

$$Z_e = 17.6 \tag{4.31}$$

but since the maximum number of teeth in mesh for a SYNCHROFLEX GENIII belt is 16, the result in 4.31 is adjusted to;

$$Z_e = 16 \tag{4.32}$$

Inserting the results from 4.27, 4.30 and 4.32 in 3.19 gives the belt width;

$$b = 16.83\text{mm} \tag{4.33}$$

Belt length and width is adjusted to one of the sizes which are available from the distributer, length is thus set to $L_b = 1215\text{mm}$ and width is set to $b = 16\text{mm}$. The width has been reduced to a smaller size then suggested in the result, but this is not a problem since according to Aratron [13], a belt with width 16mm can transmit a maximal tangential force of $F_T = 1002\,\text{N}$. Comparing this with 4.27 and 4.28 suggest that this belt is sufficient.

Regarding the results obtained above the belt chosen is a SYNCHROFLEX 16 AT3GENIII/1215. This type of belt has 405 teeth, which according to table 1 and by inserting the results from 4.27 and 4.28, implies that the pre-tension force is:

$$F_{pt\tau} = 439.8\text{N} \tag{4.34}$$

$$F_{ptP} = 449.0\text{N} \tag{4.35}$$

Further inserting these results in 3.21 gives the distance which the belt should be pulled to achieve the desired pre-tension force:

$\delta_\tau = 98.5\text{mm}$ (4.36)

$\delta_P = 96.5\text{mm}$ (4.37)

4.4 Simulations

Simulations have been done using static structural in ANSYS Workbench and are considered to be the numerical solutions for the stress and deformation calculations done on the axis and horizontal beam. The part considered in the simulation, is the top part of the vertical beam, where the axis, bearings and complete structure of phase 2 are isolated. Thus, details such as the motor which is attached at the top of the beam are not considered. Boundary conditions are presented in Appendix B-1 while the results will be presented in this chapter.

Figure 14 below shows the deformation of the axis, while figure 15 shows the deformation of the beam, which depends on the direction. In this case positive direction is upwards, while the deformation is downwards, thus the maximal absolute deformation occurs at the end of the beam, presented in 4.38. Results in both figures are expressed in meters.

$|\delta_{beam}| = 2\text{mm}$ (4.38)

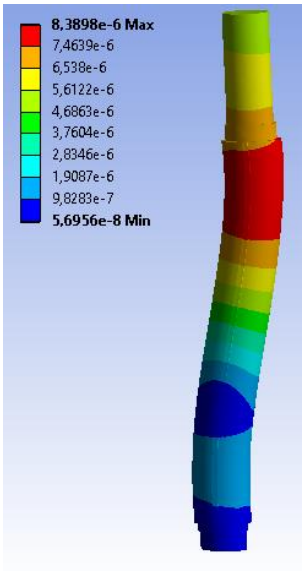

Figure 14. Total deformation for the axis, simulation results.

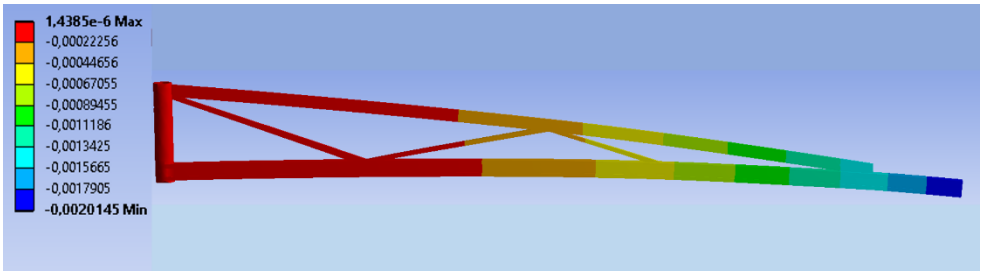

Figure 15. Directional deformation for the beam, simulation results. Positive direction is up.

Results regarding the equivalent von Mises stress are shown in figure 16 for the axis. In figure 16a the whole axis is shown, while in 16b the details are displayed. To the left in 16b is the top view of the axis, here it can be seen that stress concentrations occur at points where the geometry changes, i.e. when the diameter changes and where the tracers have been placed. The corner between the guideline and surface is a point where maximal stress occurs on the axis.

On the right side of figure 16b is the bottom part of the axis, here the stress levels are not as large as on the top side. However, there are still some regions where stress concentrations occur, these are located at the contour or near points where the geometry changes abruptly. It is noteworthy to point out that the same legend is used throughout figure 16, namely the one seen in the corner of 16a.

Stress results for the beam are shown in figure 17. Here the maximum stress was labelled in the figure with Max., since it is a stress concentration and might be difficult to spot.

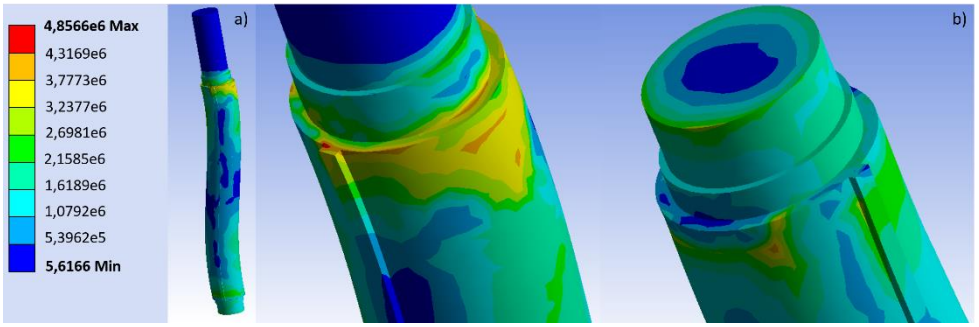

Figure 16. Stress results from the simulation regarding the equivalent von Mises stress. a) shows the whole axis, while b) shows the top and bottom part (from left to right). The legend in a) is valid for the whole figure.

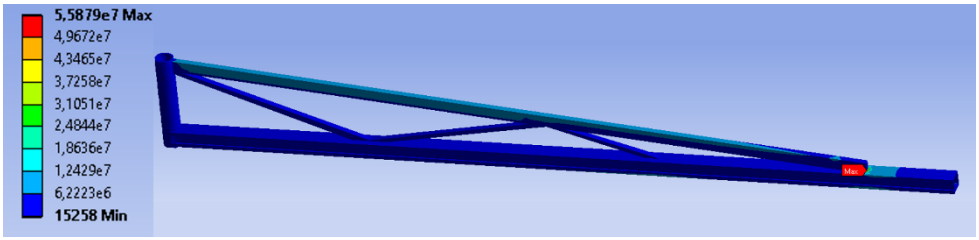

Figure 17. Results from stress simulation regarding the beam. Stress concentration with maximum stress is marked with Max. in figure.

There were restrictions on the number of elements and nodes that can be used in the simulations, the numbers used are presented in table 7.

Table 7. Number of elements and nodes in the current mesh used in the simulation.

Unit type	Number
Elements	74974
Nodes	133204

5 Discussion

5.1 Design

The philosophy behind this design was to preserve as much as possible of the parts used to create the crane. Changes were made for technical reasons only, i.e. reducing stress, and the design process involved more dimensioning then actual shape design. Hence, the reason why no conceptual phase was mentioned in the design process. However, this does not imply concepts were unused entirely, some different solutions were derived but discarded because they were impractical.

One such possible solution did not involve an axis which goes between the plates of the vertical beam, instead the phase 2 part was fastened with smaller pins at the top and bottom of the vertical beam, where the bearings are located (see figure 9). However, this solution results in an unstable phase 2, since the contour is not closed. If compared to figure 11, the cylinder will be removed, resulting in an open outer contour which reduces the stiffness of the part. This can be solved by placing a bar between the two beams, thus closing the contour of the part and increasing the stiffness. The bar is placed a bit further in, preventing it from colliding with the vertical beam, see Appendix B-2 for an illustration.

This alternative design proposes a different solution, which if compared to figure 1 and the inertia calculations done on the current design, equations 3.8-3.11, is not a better solution. The alternative has a larger inertia, since the bar closing the contour is further away from the axis of rotation, resulting in larger inertia. A larger inertia will result in a larger torque required to rotate the axis, which in turn could require a larger motor to drive it. This would increase the expenses and consequently this solution was discarded.

There is a notable difference between the structures in figure 1 and the final result in figure 13, and with concern to the discussion above, the question regarding the inertia might rise. The main elements which contribute to larger inertia is the width of the object and the distance from the axis of rotation. The beam which moves in the z-direction (up and down), is relatively thin compared to its distance to the axis of rotation, thus the contribution is not much different from the one derived in figure 1 and equation 3.11. It might also be noteworthy to mention that no results are presented for the inertia calculations since they were never conducted. The formulas were only used to get an idea of how the structure will behave during rotation.

5.2 Assembly

There was one condition which was set on the crane; enable reversible assembly. This conditions states that after assembling the crane and operating it, the crane can be disassembled again, something which is useful during transportation. Some parts are welded, such as the beams and cylinder which compose phase 2. Welds are irreversible, however there is no need for complete disassembly and since the parts in phase 2 create a neat structure, no bits are sticking out, the weld is an acceptable solution. The second phase can then be considered as a whole part, which is attached to the vertical beam. Additionally, the robot which is placed on the phase 2 beam is put on rails, which it slides on and is easy to remove, therefore this process cannot be considered irreversible.

Regarding the vertical beam and phase 1 of the design, the axis and bearings are removable, by a process which is described in section 4.2. The motor and tension adjuster are put in place by screws, which can be removed. The main concern here becomes in which way the pulleys are attached to their respective axis. According to Aratron [13], there are two ways in which the pulleys can be attached, either by placing a borehole on the surface of the pulley and fastening it with a screw. Or by buying a pulley with a guide cut out, which requires tracers on the axis if the two are to be connected. However, the second option allows movement in the axial direction, something which is not acceptable and prevented by the first, therefore the first option is chosen. With concern to the discussion above, it is concluded that the crane can be disassembled and the condition stated at the beginning of this section is fulfilled.

5.3 Bearings

Two types of bearings will be combined to create a set, as mentioned previously. The two types proposed for this solution have different outer diameters, something which might cause a problem. This implies that the bearings will need to be fitted in a housing before they are placed in the beam. The housing will keep them in place, especially the smaller one, and does not need to be much larger than the largest bearing.

Doing all of this additional work complicates the process, and since the total basic static loading coefficient is much larger than the required one, compare equations 4.25 to 4.23, the need for two bearings becomes questionable. A safety factor of 2 is used, as suggested by SFK [14] for this type of problem, which should be enough. However, there are still some uncertainties in the calculations, the results differ if comparing 4.23 to 4.24, and the difference is notable. The static load coefficient for only one bearing is barely above the limit (see C_0 for SKF 6012) and due to the

uncertainty in the results it might be better to select a larger bearing. But the larger bearings require a larger plate since the thickness of the bearing increases. The plate in question is welded to the vertical beam, see figure 9, note however that the beam has already been fitted with a thicker plate in this figure.

For the beam in the workshop at IKDC, the plate is about 10mm thick and there is no bearing available at SKF which can fit into this plate and meet the requirements for the static loading factor. Therefore, the plates will have to be replaced nevertheless, and since they are already being replaced the possibility to attach larger plates which can fit larger bearings becomes an option. Due to the reasons stated above, it is considered a good idea to replace the plates on the beam with thicker ones.

Considering the uncertainties in the calculations it will be reasonable to choose a bearing with a static loading coefficient of $C_0 \approx 30$kN. However, the bearing in the catalogue which matches these requirements is heavier and larger than if two smaller bearings would be fitted instead. Hence, the reason why two bearings were chosen.

Due to the simplicity of the assembly, it is easy to replace the phase 2 part with some other part which can take a heavier load. The stress calculations and simulations suggest that the axis and bearings are capable of carrying a heavier load. Therefore, the possibility of making this adjustment without causing failure in the bearings or axis, exist.

5.4 Transmission

Belt width was calculated using 4.27 which is the normal tangential force obtained from the motor torque. This could also be done using the normal tangential force obtained from the motor power output and comparing 4.28 to 4.27, it is obvious that these two calculations do not yield the same force. However, if 4.28 is used in 3.19, the new belt width will not differ much from the result obtained in 4.33. This implies that the choice of tangential force calculation is arbitrary and the difference between the obtained results is neglectable. The main reason why two equations are presented is in case only one variable of the two is known, e.g. the torque is known but not the power. Then the calculations can still be done without the complete knowledge of the motor specifications, but since this is not the case in the current situation, the choice becomes arbitrary.

In the present calculations, the force obtained through the torque is used, which is slightly larger than the one obtained from the power. This might act as an extra safety to ensure that the belt is not overloaded. However, this should not be a problem for the current belt, since data suggests that the maximum allowed tangential force in the belt is much larger than the force currently present.

The distance which the belt should be pulled to achieve a desirable pre-tension force, might be a bit too long. As suggested by the calculations 4.36 and 4.37, the belt must be pulled a distance of approximately 90mm. This is quite long and the error might be in the Young's modulus for the belt, obtained from Vedmar [12]. The belt used by Vedmar might be a different one than the one used in this situation, thus these results might have to be applied with care. Since the belt provider has not given any information about the material composition of the belt, the modulus suggested by Vedmar is the best available approximation to go by.

5.5 Solid mechanics

The deformation results which were obtained in 4.2-4.5 and 4.38, all suggest that the deformations are relatively small. Larger deformations occur at the end of the horizontal beam, but even those are limited to a few millimetres, which is acceptable considering the overall dimensions of the beam. Furthermore, the stresses obtained are also bellow the yield stress for the material, which is $\sigma_y = 355\text{MPa}$ for the axis and beams, see 4.8-4.11, 4.13-4.16 and 4.18 for calculations and figures 16 and 17 for simulation results. The largest stress is found in the weld but is still below the maximum allowed stress.

It has already been mentioned that the weld calculations are done on a weld which hold the whole ZP-I beam by itself, thus no supports. This suggests that the stress in the weld might be larger than what it would be if the supports are added to help carry the beam. But this also provides a good method to ensure that the weld is sufficient and will not result in failure, since if a larger load can be carried then a smaller one should provide no problem.

Fatigue is branch of science which falls under the term solid mechanics, and is often considered in moving parts with cyclic varying load. Even though the maximum applied load is well below the limit, parts might yield after some time. However, no calculations were done to check for possible failure due to fatigue, this is because the parts do not move as much. The axis might be a part which is prone to fatigue failure, but since it does not do complete revolutions, the load applied to the axis cannot be considered varying but is instead a concentrated load to one side of the part. This is the same reason why the bearings are considered static and consequently fatigue is ignored.

Due to the fact that the calculated stresses are way below the yield stress of the material, no additional attention was given to safety. Initially the beams were planned to be dimensioned so that the maximum stress is half the yield stress, but this will not be necessary.

However, the current results suggest that the crane is over dimensioned and that a smaller structure could be made in order to save resources. But this is not possible

since most of the parts used are already available at the workshop at IKDC. E.g. the cross section of the ZP-I beam is 80x80mm, if it is welded to an axis, the axis needs to have a cross-section diameter of at least 90mm to fit the beam. To get more use out of the components, a larger load might be applied, but there are restrictions in how much the robot from Güdel can carry. Hence, there is no choice but to accept an over dimensioned crane, which might not be all bad since if e.g. the robot is replaced, the crane could carry a larger load. This gives more freedom for future modifications. Yet, there is a benefit with some parts being over dimensioned, one of them is the axis. The bottom bearings are kept in place mostly because of the weight of the axis which pushes down on them. This prevents movement in the axial direction and also prevents the axis from possibly jumping out of place.

Comparing figure 3, which was used to derive the theory for the calculations, to figure 11, showing the result of the final design, notice that the latter is an up-side-down version of the first figure. Still, this difference does not affect calculations, since they are independent of the direction, the material is linear elastic and independent of the direction from which the load is applied.

Comparisons between the analytical, semi-analytical and numerical (simulation) results will be discussed in separate sub-sections below. Here the validity of the different methods will also be discussed as well as the advantages and disadvantages.

5.5.1 **Analytical**

The analytical results are seen in 4.2 and 4.4 for the deformation of the beam and axis respectively. Stress results for the two beams are presented in 4.8 and 4.9, while the maximum stress for the axis is shown in 4.14. Comparing the analytical results with the others, deformation and stress only, the analytical methods yield results which are larger i.e. larger deformation and larges stresses. The analytical method is based on approximations and assumptions which make the calculations easier and can be solved with simple tools, such as a pocket calculator. These methods also rely on tabulated data which are case specific, i.e. the elementary cases, but as shown in chapter 3.4, these cases can be applied to more general problems with superposition. Hence, it is important to use correct approximations and assumptions when applying this method, inaccuracy in the results is a sign of bad assumptions.

Since the analytical methods give results which are larger, they can be considered more conservative than the semi-analytical. Analytical methods are also more prone to human errors, which is the biggest disadvantage with this method. If the number of variables is big, the equations can become tedious and thus a small mistake can have huge consequences which might be difficult to spot. The difference between analytical and semi-analytical results varies, but even when the difference is big such as in 4.8 and 4.10, where 4.8 is four times larger, the physical difference is not

that large, ~40MPa. This suggests that the accuracy of the analytical methods is good compared to the semi-analytical methods.

The fact that analytical methods have been around for years, before any numerical methods were developed, such as FEM, suggest that they are very reliable. There is nothing wrong with the method, only the mistakes which the engineer can do during calculations. However, results obtained by the analytical- and semi-analytical method agree with each other to some extent, in some cases more than in others, which proves that the assumptions used in these calculations are correct. The results obtained by the analytical method might be seen as a more conservative solution of the current problem.

5.5.2 **Semi-analytical**

The results obtained by the semi-analytical method are seen in 4.3, 4.5, 4.10, 4.11 and 4.16. As mentioned in section 3.4, the semi-analytical method uses the same equations for stress calculations as the analytical. Only deformations can be directly obtained in CALFEM, which was only done for the horizontal beams of phase 2. The reason for this is the varying cross-section of the axis, which would require a more detailed mesh. However, it was proved in section 4.3.1 that the deformations directly derived given by CALFEM and the ones calculated using the analytical expressions, yield the same result. The reason for this is that CALFEM is based on the same methods and therefore should theoretically yield the same results. Therefore, there is no need to spend time on defining a complicated mesh for the axis.

The main advantage with CALFEM is the simplicity by which a problem can be solved. There is no need to keep track on tedious equations and the unknown forces, i.e. reaction- and inner forces can be calculated with ease. Additionally, user defined boundary conditions can be applied, which removes the error related to finding appropriate elementary cases to approximate the boundary conditions with. In the current problem, the boundary conditions are quite unusual due to the bearings, since they might be considered as fastened, but result in no reaction moments, unlike something a tightly fastened beam would do.

Furthermore, the semi-analytical method provides the reaction forces and inner forces as point forces, which is an advantage if the results are used in conjunction with analytical methods, such as in this case. This also provides a neat way to check the results obtained by the man-solved equations. If any mistakes were made by the engineer, they would be noticed when compared to the result obtained from CALFEM.

The disadvantage with the semi-analytical method is the mesh. Even though the user defined mesh allows more control of the solution and results can be directly obtained at the nodes, the mesh might be difficult to create. This is the case for the axis which

is the reason why no mesh was created at all. Thus, for a complicated geometry, creating the mesh becomes a tedious and time-consuming work. Additionally, this method does not account for stress concentrations, which must be adjusted for by using the equation 3.51.

In conclusion; the semi-analytical method provides an easy way to check the analytical results. For a simple geometry, the method gives fast results and allows for user defined boundary conditions, which enables the application of this method to complex problems. The results obtained by this method are assumed to be very accurate since the method relies on proven theory and removes the human-error factor.

5.5.3 **Simulations**

Figures 14, 15, 16 and 17 show the results from the simulation (numerical method) done in ANSYS. The simulation uses FEM theory, which is similar to CALFEM, but because it is a commercial software, a black box situation exists where complete knowledge behind the computation is not known. However, the different options are explained and how to apply them so that the desired conditions are obtained during simulation. E.g. bearing support conditions can be applied directly to a surface.

Another detail which is important to pay attention to when conducting FEM simulations, is how contacts are modelled, especially when performing simulation on an assembly of different parts, such as in this case. The contact formulations describe the stiffness and how contacts are modelled, e.g. how much do the surfaces deform and if one surface is allowed to penetrate the other. In this situation, the standard contact formulation was used, which states that displacements are tied together at the surface, i.e. two bonded surfaces will deform equally. If modelled wrong, the contacts might be a source of error and since detailed information about the contacts are not known, the standard formulation was used to avoid errors.

However, the biggest advantage with using ANSYS is that the mesh is autogenerated, only mesh size and position must be specified as compared to CALFEM where the mesh is created manually. The automatic mesh saves a lot of time and gives a more detailed mesh than what could be done with CALFEM. This in turn results in accurate solutions which account for stress concentrations due to the details in the mesh. Same accuracy could theoretically be obtained with CALFEM, since the methods used are the same, but due to the complications in creating a fine mesh, it becomes impractical for complicated geometries. But owing to this, the simulations become too mesh dependent, and it is necessary to create a fine mesh in order to get the most accurate results. Yet, mesh size increases computational time and it becomes a trade-off. Nevertheless, results are prone to converge and at some point, a finer mesh will not give better results.

The results obtained from the simulation differ notably compared to the ones obtained from the analytical and semi-analytical solutions, the simulation results are much lower regarding stresses and deformations. This might be due to the fact that a size limit was put on the mesh, which has to do with the software license. The maximum stress in the result increases as the mesh gets refined, see Appendix B-3 for a simulation of the phase 2 part when a coarser mesh is used. Thus, it is possible that the results would converge with the semi-analytical if a finer mesh was used.

To limit the mesh dependency of the simulation, separate solutions were made for the beam and axis. As mentioned previously, an assembly of the top part was used in ANSYS, as an attempt to try to model the connections more accurately. But a separate mesh was created when simulations were done on each part, e.g. when simulations were done on the axis, the axis had a finer mesh than the rest of the assembly, with the mesh getting coarser further away from the object considered. This way, the axis and connecting parts would be modelled more accurately and the possibility of identifying stress concentrations increases. Nevertheless, the results are not as good as if a refined mesh was used for the complete assembly.

The reason why a simulation was performed was to check the validity of the analytical, and semi-analytical results, to ensure that they are correct. In order to do so, the simulation must be similar to the previous methods, otherwise different results will be obtained for each method. In the previous method, the load was modelled as a point force, which would yield larger stresses than an evenly distributed load across the whole beam. However, as mentioned previously, point forces cannot be modelled in ANSYS, but instead load is applied to a surface. To compensate for this and obtain a load more similar to a point load, a very small surface was made at the end of the beam, at which the load was applied.

According to the discussion above, the simulation might come off as useless, due to its lack of accuracy, stress results are more inaccurate than deformation. But important knowledge might still be drawn from the results. Firstly, the results confirm that the stresses and deformations are well below what is allowed for the structure. Secondly, the deformation results show how the beam and axis deforms, note that the deformations were exaggerated in figures 14 and 15. This might act as a tool to confirm if the assumptions made in section 3.4.1, during the derivation of the analytical method, are correct.

5.6 Conclusion

A crane which will be used for additive manufacturing of buildings was designed from parts at the IKDC workshop. The proposed design of the crane is shown in figure 13 as a 3D CAD drawing. Some parts were modified, such as the vertical beam where new plates were fixated, together with a new axis. Bearings of type SKF 6012 and 16013 were paired and placed at the top and bottom of the beam.

Furthermore, a motor of type QSY 130 C EcoDyn, was placed on an adjuster unit at the top surface of the vertical beam. Torque is transmitted from the motor to the axis through a toothed belt of type Synchroflex AT3GENIII, with length 1215mm and width 16mm.

The other parts are a beam of type ZP-I, which is cut in two, and a robot which is placed on racks, on the beams. One of the beams was fitted with supports and welded to a hollow cylinder, which enables it to be fastened to the axis of the vertical beam.

Stress and deformations were calculated using analytical, semi-analytical and numerical methods. The results from all three methods were compared were it was concluded that the semi-analytical method gives the most accurate results, due to the fact that it is insensitive to human errors done during the derivation of forces. The analytical method is also equally accurate in theory, but is considered as a conservative solution in the current case. All three suggest that the stresses are well below the yield stress of the material and that the structure might be over dimensioned. However, nothing can be done about this fact since the parts used are quite large from the beginning and are limited by the robot who cannot carry a heavier load. The current load is set to 125kg.

Calculations were also done on the weld to ensure that it holds, the results show that the weld is sufficient to carry the beam for the current load and without supports. Thus, with supports the upper limit of the load might be increased, but a more detailed analysis should be conducted if increasing the load limit is considered.

The crane was not assembled at this current state, but the assembly process is left as part of a possible future project. This could be done be either students as part of a course or by the department, whichever the department seems more fit. Control of the motors was not considered either in this work but is left as something which can be done in the future.

References

[1] The construction of Europe's first 3D-printed building has begun. (2015). Retrieved March 20, 2018, from https://3dprinthuset.dk/europes-first-3d-printed-building/

[2] Starr, M. World's first 3D-printed apartment building constructed in China. (2015). Retrieved March 20, 2018, from https://www.cnet.com/news/worlds-first-3d-printed-apartment-building-constructed-in-china/

[3] Introducing BOD2. (n.d.). Retrieved March 20, 2018, from https://3dprinthuset.dk/3d-construction-printer/

[4] Güdel Product Catalogue. (n.d.). Retrieved March 14, 2018, from https://gudel.picturepark.com/Website/Download.aspx?DownloadToken=d3de035d-4568-42aa-8abe-1d9d033399fb&Purpose=AssetManager&mime-type=application/pdf#page=30

[5] Lim, S., Buswell, R.A., Le, T.T., Austin, S.A., Gibb, A.G.F. & Thorpe, T. (2012). Developments in construction-scale additive manufacturing processes. *Automation in Construction, 21*(1), 262-268. https://doi.org/10.1016/j.autcon.2011.06.010

[6] Wu, P., Wang, J. & Wang, X. (2016). A critical review of the use of 3-D printing in the construction industry. *Automation in Construction, 68*(1), 21-31. https://doi.org/10.1016/j.autcon.2016.04.005

[7] Labonnote, L., Rønnquist, A., Manum, B. & Rüther, P. Additive construction: State-of-the-art, challenges and opportunities. *Automation in Construction, 78*(1), 347-366. https://doi.org/10.1016/j.autcon.2016.08.026

[8] WinSun Company Profile. (n.d.). Retrieved March 21, 2018, from http://www.winsun3d.com/En/About/

[9] Woollaston, V. & Steadman, I. (2017). The race to build the first 3D-printed building. Retrieved March 21, 2018, from http://www.wired.co.uk/article/architecture-and-3d-printing

[10] Austrell, P. E., Dahlblom, O., Lindemann, J., Olsson, A., Olsson, K. G., Persson, K., Ristinmaa, M., Sandberg, G. & Wernberg, P. A. CALFEM: A Finite Element Toolbox, Version 3.4. (2004). Lund, Sweden, Department of Structural Mechanics, Lund University.

[11] Meriam, J. L. & Kraige, L. G. (2013). *Engineering Mechanics Dynamics* (7th ed.). New York, USA: Wiley.

[12] Vedmar, L. (2014). *Transmissioner* [Transmissions]. Lund, Sweden, Department of Machine elements, Lund University.

[13] Aratron Product Catalogue. (2016). Retrieved January 9, 2018, from https://www.aratron.se/wp-content/uploads/2016/05/15-717_Aratron_Kuggremskatalog_2016_webb.pdf

[14] SKF. (2014). SKF Product catalogue. Sweden, SKF-group.

[15] Ljung, C., Ottosen, N.S. & Ristinmaa, M. (2014). *Introduktin till hållfasthetslära, enaxliga tillstånd* [Introduction in Solid Mechanics, uniaxial state conditions]. Lund, Sweden: Studentlitteratur.

[16] Vedmar, L. & Jacobson, B. (2015) *Tribologi* [Tribology]. Lund, Sweden, Department of Machine elements, Lund University.

[17] Ottosen, N.S., Ristinmaa, M. & Ljung, C. (2014). *Hållfasthetslära, allmänna tillstånd* [Solid Mechanics, general state conditions]. Lund, Sweden: Studentlitteratur.

[18] Ottosen, N.S. & Petersson, H. (1992). *Introduction to the Finite Element Method*. Lund, Sweden, Prantice Hall.

[19] MITCalc Weld Connections. (n.d.). Retrieved March 28, 2018, from http://www.mitcalc.com/doc/welding/help/en/welding.htm

[20] European Committee for Standardization (EN). (2005). *Design of steel structures – Design of joints* (EN-1993-1-8). Brussels, Belgium: European Committee for Standardization (EN).

[21] Sundström, B. & Alfredsson, B. editor. (2014). *Handbok och formelsamling i Hållfasthetslära* [Tables and formulas in Solid Mechanics]. Stockholm, Sweden, Department of Solid Mechanics, KTH.

[22] Heidenhain QSY 130 EcoDyn. (n.d.) Retrieved January 15, 2018, from https://www.heidenhain.se/sv_SE/produkter/styrsystem-foer-verktygsmaskiner/servoteknologi/synkronmotorer/qsy-130-ecodyn-series/

Appendix A Time plan

A.1 Project plan and outcome

The planned timeline is presented in figure A-1, as seen here the work is divided into three parts, the two phases and a finalization phase where the different parts are brought together. Each of the two phases are structured in a similar manner, a design is proposed and then calculations are done. The phase is ended with creating a CAD drawing of the design and conducting FEM simulations. The presentation date was expected to be in early May.

However, everything did not go as planned and some changes were made. I attended a course between January and March, which delayed the progress a bit. But I managed to catch up the time I lost after the course was finished. Furthermore, the presentation date for the whole department is in June, which leaves more time to perfect the work and report. The outcome is presented in figure A-2.

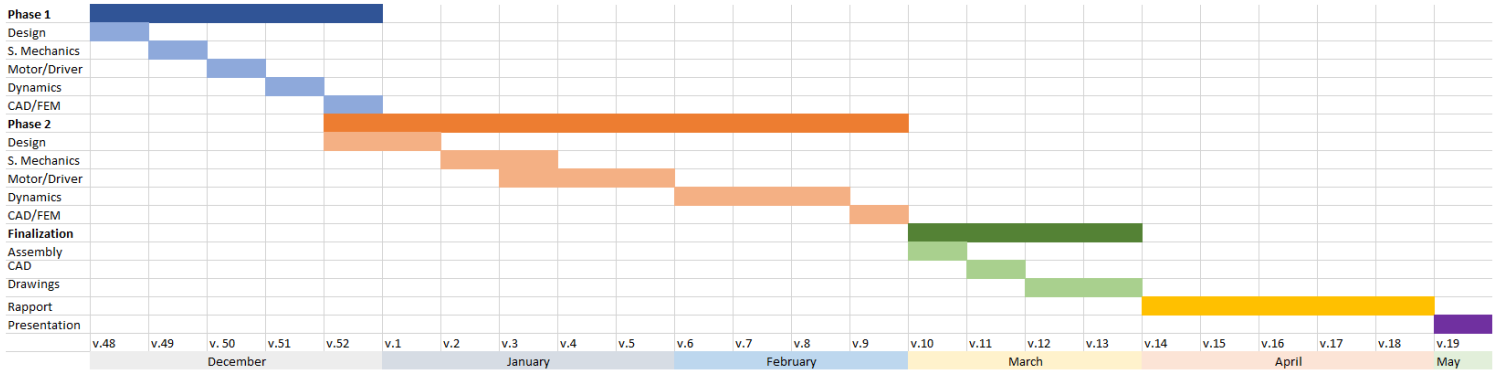

Figure A-1. Planned time schedule for the work.

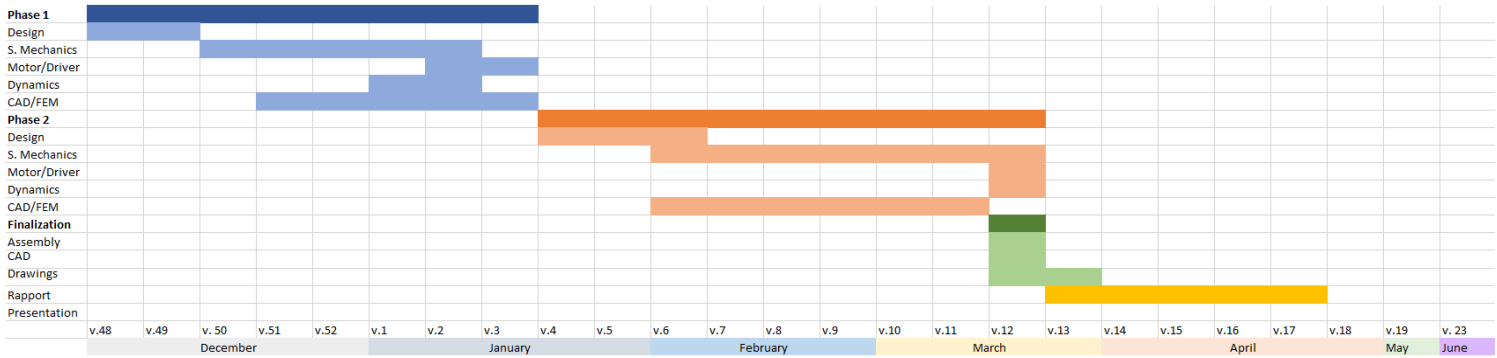

Figure A-2. Work and time distribution of the actual outcome.

Appendix B CAD & FEM

The boundary conditions used during the simulation are shown in figure B-1. Here a fixed support was placed at the base, while a force was applied to a small surface at the end. A small surface was chosen in order to represent a point force load. Furthermore, additional CAD drawing and FEM results are shown, which were not presented in the result. Figure B-3 shows the stress results for a coarser mesh and in figure B-2 an alternative design of phase 2 is presented.

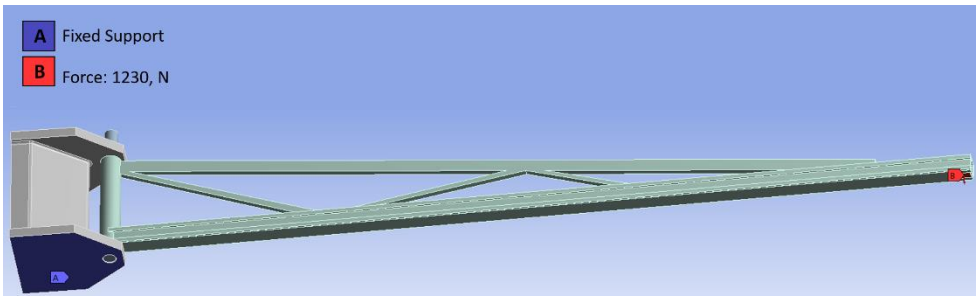

Figure B-1. Boundary conditions used during the FEM simulation. Fixed support at the bottom of the beam and a force is applied to a small surface, in an attempt to model point force load.

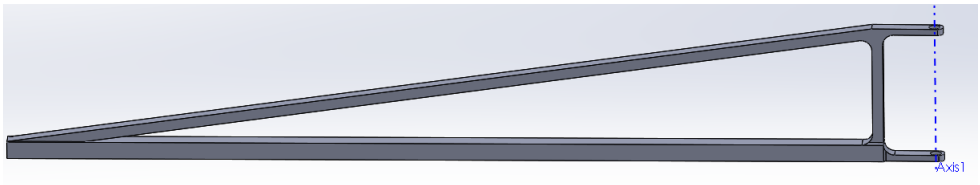

Figure B-2. 3D CAD drawing for the alternative solution of phase 2.

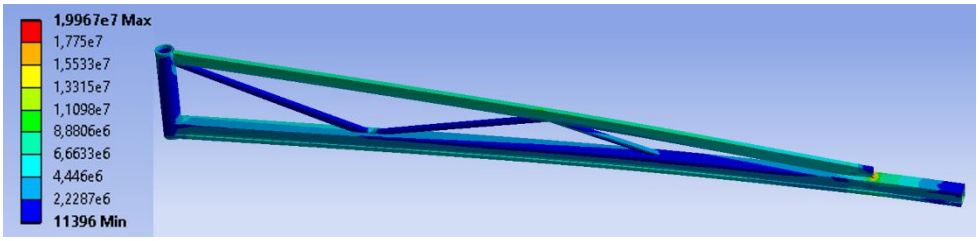

Figure B-3. Stress results from FEM simulation for a coarser mesh than the one used in the final result.

Appendix C CALFEM code

The CALFEM code use in the MATLAB script is shown below.

```
%% CALFEM

E = 2.1e11;                          %Young's modulus
%Custom square-beam, h = 30 mm, b = 30mm
A1 = (0.03*0.03)-(0.018*0.018);
%80x80 ZP-I hollow square
A2 = (0.08*0.08)-(0.0674*0.0674);
%Inertia of square-beam

I1 = (0.006*(0.03^3)/6)+(0.5*0.006*(0.03^3));
I2 = 189/(100^4);                    %Inertia ZP-I beam
P = 125*9.81;                        %Load

Edof = [1 1 2 3 4 5 6;
         2 7 8 9 4 5 6];

Ex1 = [0, 4];
Ex2 = [0, 4];
Ey1 = [0.5, 0.5];
Ey2 = [0, 0.5];

ep1 = [E A1 I1];
ep2 = [E A2 I2];

K = zeros(9);                         %Empty stiffness matrix
f = zeros(9, 1);                      %Load matrix
f(5) = -P;                            %Applied load at node 5

Ke1 = beam2e(Ex1, Ey1, ep2);          %Element stiffness
Ke2 = beam2e(Ex2, Ey2, ep1);

K = assem(Edof(1,:), K, Ke1);         %Global stiffness matrix
K = assem(Edof(2,:), K, Ke2);

bc = [1 0; 2 0; 3 0; 7 0; 8 0; 9 0]; %Boundary conditions
```

```
[u, R] = solveq(K, f, bc);              %Deformations &
reaction forces

Ed = extract(Edof, u);
%Inner forces for ZP-I beam
es1 = beam2s(Ex2, Ey2, ep2, Ed(1,:));
%Inner forces for square-beam
es2 = beam2s(Ex2, Ey2, ep1, Ed(2,:));
```